

Motion Detection in Diffraction Tomography by Common Circle Methods

Michael Quellmalz* Peter Elbau† Otmar Scherzer†‡§ Gabriele Steidl*

September 19, 2022

Abstract

The method of common lines is a well-established reconstruction technique in cryogenic electron microscopy (cryo-EM), which can be used to extract the relative orientations of an object in tomographic projection images from different directions.

In this paper, we deal with an analogous problem in optical diffraction tomography. Based on the Fourier diffraction theorem, we show that rigid motions, i.e., a map composed of rotations and translations, can be determined by detecting common circles in the Fourier-transformed data.

We introduce two methods based on the idea of identifying common circles to reconstruct the object motion: While the first one is motivated by the common line approach for projection images and detects the relative orientation by the shape of the common circles in the two images, the second one assumes a smooth motion over time and calculates the angular velocity of the rotational motion from an infinitesimal version of the common circle method.

Interestingly, using the stereographic projection, both methods can be reformulated as common line methods, but these lines are, in contrast to those used in cryo-EM, not confined to pass through the origin and allow for a full reconstruction of the relative orientation.

Numerical proof-of-the-concept examples demonstrate the performance of our reconstruction methods.

Keywords. Diffraction tomography, motion detection, Fourier diffraction theorem, common circle method, optical imaging.

Math Subject Classifications. 92C55, 78A46, 94A08, 42B05.

1 Introduction

A key task in many imaging modalities consists in recovering an object's inner structure given images of its illuminations from different directions. The *X-ray computed tomography* (CT) is based on a number of assumptions, most prominently that the light travels along straight lines. If, however, the object is small compared to the wavelength of the illumination, the optical diffraction cannot be neglected anymore. This occurs for example when examining structures with a size of a few micrometers such as biological cells with visible light. In the so-called *optical diffraction tomography*, we respect the wave character of the light and take optical diffraction into account.

*TU Berlin, Straße des 17. Juni 136, D-10587 Berlin, Germany, {quellmalz, steidl}@math.tu-berlin.de.

†University of Vienna, Oskar-Morgenstern-Platz 1, A-1090 Vienna, Austria, {otmar.scherzer, peter.elbau}@univie.ac.at

‡Johann Radon Institute for Computational and Applied Mathematics (RICAM), Altenbergerstraße 69. A-4040 Linz, Austria

§Christian Doppler Laboratory for Mathematical Modeling and Simulation of Next Generations of Ultrasound Devices (MaMSi), Oskar-Morgenstern-Platz 1, A-1090 Vienna, Austria

As biological samples should be imaged preferably in a natural environment, contact-free manipulation methods are used for rotating the object during the image acquisition process. Such rotations can be induced by optical [13] or acoustical tweezers [6, 21, 32], where especially the latter often provide less accurate control of the motion.

Therefore, additional effort is necessary if the rigid motion of the object during the image acquisition process is unknown and has to be reconstructed from the captured images. In this paper, we propose to tackle this problem by a new method of common circles and its infinitesimal version which is inspired by the well-known method of common lines for projection images as applied in cryogenic electron microscopy (cryo-EM) [30, 33, 35]. Let us briefly recall this method first.

Method of common lines. In computed tomography, the aim is the reconstruction of an object from given (optical) projection images for different directions of the imaging wave or, equivalently, different rotations of the object. The object's absorption properties are described by a function $f: \mathbb{R}^3 \rightarrow \mathbb{R}$, which has to be recovered. We assume the object moves in time t according to rotation matrices R_t , and the illumination is in direction $e^3 = (0, 0, 1)^\top$. Then, the *ray transform* of f is given by

$$\mathcal{X}_{R_t}[f](x_1, x_2) := \int_{-\infty}^{\infty} f\left(R_t(x_1, x_2, x_3)^\top\right) dx_3, \quad (x_1, x_2)^\top \in \mathbb{R}^2. \quad (1.1)$$

The reconstruction of f is based on the Fourier slice theorem, see e.g. [26, Theorem 2.11], which states that

$$\mathcal{F}^{(2)}[\mathcal{X}_{R_t}[f]](k_1, k_2) = \sqrt{2\pi} \mathcal{F}^{(3)}[f](R_t(k_1, k_2, 0)^\top), \quad (k_1, k_2)^\top \in \mathbb{R}^2, \quad (1.2)$$

where $\mathcal{F}^{(2)}$ and $\mathcal{F}^{(3)}$ denote the two- and three-dimensional Fourier transforms, see (2.9). Hence, given the data $\mathcal{X}_{R_t}[f]$ for the rotation R_t , we obtain the Fourier transform of f on the plane $P_{R_t} := \{R_t(k_1, k_2, 0)^\top : (k_1, k_2)^\top \in \mathbb{R}^2\}$ through the origin. If the rotations R_t are known and the planes P_{R_t} fully cover \mathbb{R}^3 , e.g. when the object makes a full turn around a fixed rotation axis other than $\mathbb{R}e^3$, then we can reconstruct f by the inverse 3D Fourier transform. However, in cryo-EM, the rotations R_t of the object are not known. The method of common lines makes use of the fact that two planes P_{R_s} and P_{R_t} intersect for $R_s e^3 \neq \pm R_t e^3$ in a common line which contains the origin. This common line can be detected from the data by maximizing a certain correlation of all possible combinations of lines in the two planes which is a minimization problem in two variables. Note that the common line detection is usually not performed directly in the Fourier space, but by comparing lines of the 2D Radon transform of $\mathcal{X}_{R_t}[f]$, see [34] and also [3] for computational methods. Keeping one plane fixed, the second plane is not uniquely determined just by their common line, see Figure 1 (left side). We have to compute the pairwise common lines between three planes to determine the rotation angles between them, see Figure 1 (right side). Alternatively, the reconstruction can be done by moment-based methods [18]. Furthermore, Kam's method considers reconstructing f without the need of computing the motion parameters first [15, 29].

Diffraction tomography. In optical diffraction tomography, we use a modeling based on Born's or Rytov's approximation of the scattered wave, see e.g. [14, Chapter 6]. The Fourier diffraction theorem [36] provides a relation between the measured (and Fourier-transformed) data and the Fourier transform of the scattering potential, which we want to reconstruct. Once we know the motion parameters, the scattering potential can be reconstructed using a backpropagation formula [5, 25] or inverse discrete Fourier methods [19], which can deal with arbitrary, irregular motions. Under Born's approximation and certain conditions on the moments of the scattering potential, it was shown [20] that there exists a unique solution to the problem of determining

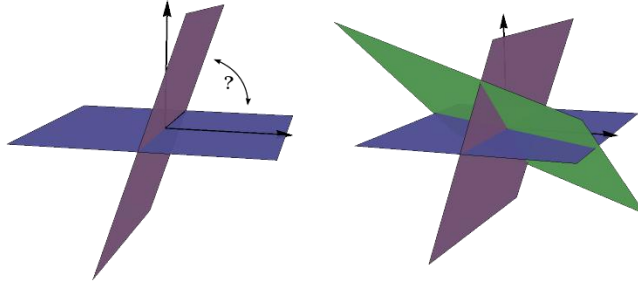


Figure 1: *Left:* A common line pair between two planes P_{R_s} and P_{R_t} does not determine the relative angle between them uniquely. *Right:* Knowing pairwise common lines between three planes, we can determine their orientations uniquely (except for degenerate cases). The two graphics are courtesy of Denise Schmutz from [28, Figure 6.2 and Figure 6.3].

the scattering potential given measurements with unknown object rotations, if they cover the whole set of rotation matrices.

In this paper, we are interested in an experimental setup where the parameters of the rigid motion need to be determined in parallel to the tomographic reconstruction. We show that the rotations can be determined by an approach which we call the “method of common circles”. It relies on the intersection of hemispheres in a common circular arc inside the Fourier domain. In particular, we show that only two hemispheres are required to compute the rotation, whereas, in the context the inversion of the ray transform based on the Fourier slice theorem, one needs to consider the intersection of three planes. Furthermore, the object’s translation can be completely determined from the measurement data, where we have to plug in the restriction that the scattering potential is real-valued, which means that the object scatters but does not absorb light. This is in contrast to the ray transform, where the measurements are invariant to every translation of the object in direction of the incident wave. The diffraction data is sensitive to the third component of the translations, which allows the full recovery. To the best of the authors’ knowledge, there is no existing work on motion detection in this diffraction tomography setting, except for the more simplified model considering only projections.

Outline of this paper. In [Section 2](#), we describe the model of diffraction tomography with the object undergoing a rigid motion. Then, in [Section 3](#), we derive the common circle method for reconstructing the object’s rotations and relate it via stereographic projection to a common line method. In [Section 4](#) we give an infinitesimal version of this common circle method, where we need to assume that the rotations depends smoothly on the time. [Section 5](#) then covers the reconstruction of the translations of the object. The numerical simulations in [Section 6](#) indicate that the reconstruction of the rigid object motion is possible, where we perform the proposed methods with two different phantoms and different motion parameters. Moreover, we see that when implementing the common circle method, we can efficiently compute a starting solution for the optimization using the infinitesimal method.

2 Diffraction Tomography

2.1 Fourier diffraction theorem

Throughout this paper, we consider the experimental setup of *optical diffraction tomography* which we will briefly describe in the following based on [19, 36]. The unknown object is illuminated by an *incoming plane wave* which propagates in direction $\mathbf{e}^3 = (0, 0, 1)^\top$ with wave number

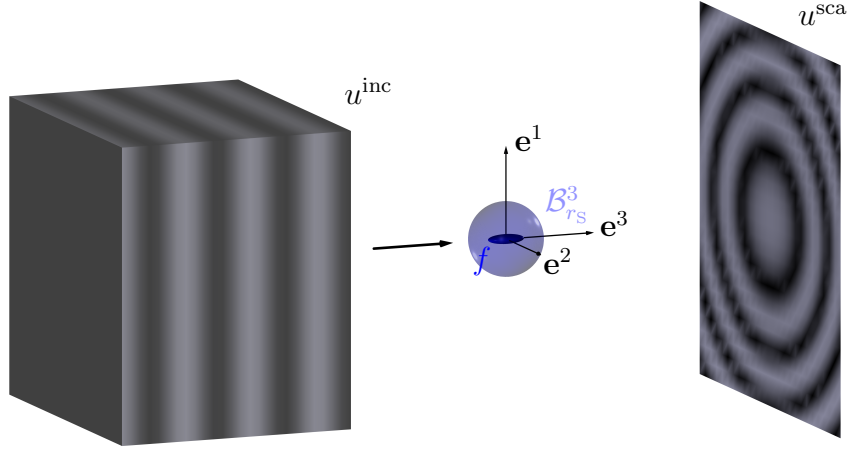


Figure 2: Experimental setup of transmission imaging in optical diffraction tomography.

$k_0 > 0$. In frequency space, this is represented by a function

$$u^{\text{inc}}(\mathbf{x}) := e^{ik_0 x_3}, \quad \mathbf{x} \in \mathbb{R}^3, \quad (2.1)$$

where we normalized the amplitude to one.

The object shall be contained in an open ball $\mathcal{B}_{r_s}^3$ for some radius $r_s > 0$, where we use the notation

$$\mathcal{B}_r^d := \{\mathbf{x} \in \mathbb{R}^d : \|\mathbf{x}\| < r\} \quad \text{for } d \in \mathbb{N}, r > 0,$$

with $\|\cdot\|$ denoting the Euclidean norm.

The incident wave u^{inc} then induces a *scattered wave* u^{sca} which is recorded in transmission imaging in a plane $\{\mathbf{x} \in \mathbb{R}^3 : x_3 = r_M\}$ at a position $r_M > r_s$ outside the object, see Figure 2. The scattered wave u^{sca} can be calculated from the incoming wave u^{inc} and the *scattering potential* $f: \mathbb{R}^3 \rightarrow \mathbb{C}$ of the unknown object as a solution of the partial differential equation

$$-(\Delta + k_0^2)u^{\text{sca}} = f(u^{\text{sca}} + u^{\text{inc}}) \quad (2.2)$$

which fulfills the Sommerfeld radiation condition

$$\lim_{r \rightarrow \infty} \max_{\|\mathbf{x}\|=r} \|\mathbf{x}\| \left| \langle \nabla u^{\text{sca}}(\mathbf{x}), \frac{\mathbf{x}}{\|\mathbf{x}\|} \rangle - ik_0 u^{\text{sca}}(\mathbf{x}) \right| = 0. \quad (2.3)$$

To guarantee a unique solution $u^{\text{sca}} \in H_{\text{loc}}^2(\mathbb{R}^3 \rightarrow \mathbb{C})$ of this equation system, see [4, Theorem 8.7], we make the (natural) assumption that f is a piecewise continuous function with

$$\text{Re } f(\mathbf{x}) \geq 0 \quad \text{and} \quad \text{Im } f(\mathbf{x}) = 0 \quad \text{for all } \mathbf{x} \in \mathbb{R}^3 \quad (2.4)$$

and with nonempty, compact support $\text{supp}(f) \subset \mathcal{B}_{r_s}^3$.

If $\|f\|_\infty$ is sufficiently small, the solution u^{sca} is small in comparison to u^{inc} , so that it can be neglected on the right-hand side of (2.2) and we obtain the *Born approximation* u of the scattered field u^{sca} , determined by

$$-(\Delta + k_0^2)u = fu^{\text{inc}}, \quad (2.5a)$$

$$\lim_{r \rightarrow \infty} \max_{\|\mathbf{x}\|=r} \|\mathbf{x}\| \left| \langle \nabla u(\mathbf{x}), \frac{\mathbf{x}}{\|\mathbf{x}\|} \rangle - ik_0 u(\mathbf{x}) \right| = 0. \quad (2.5b)$$

In the following, we assume that the Born approximation of the scattered wave is valid, which holds true for small objects which are mildly scattering, cf. [8, 14].

The advantage of the Born approximation is that the solution $u \in H_{\text{loc}}^2(\mathbb{R}^3 \rightarrow \mathbb{C})$ of the Helmholtz equation (2.5a) fulfilling the radiation condition (2.5b) can be explicitly written in the form

$$u(\mathbf{x}) = \int_{\mathbb{R}^3} \frac{e^{ik_0\|\mathbf{x}-\mathbf{y}\|}}{4\pi\|\mathbf{x}-\mathbf{y}\|} f(\mathbf{y}) u^{\text{inc}}(\mathbf{y}) \, d\mathbf{y},$$

see, for example, [4, Theorem 8.1 and 8.2].

To calculate from the detected field $u(x_1, x_2, r_M)$, $(x_1, x_2) \in \mathbb{R}^2$, the scattering potential f , we use the Fourier diffraction theorem, which relates the two-dimensional Fourier transform of the measurement $(x_1, x_2) \mapsto u(x_1, x_2, r_M)$ to the three-dimensional Fourier transform of the scattering potential f , see for instance [14, Section 6.3], [26, Theorem 3.1] or [36]. We use here the version [19, Theorem 3.1] derived for the more general case $f \in L^p(\mathbb{R}^3 \rightarrow \mathbb{C})$, $p > 1$, which states that

$$\mathcal{F}_{1,2}[u](\mathbf{k}, r_M) = \sqrt{\frac{\pi}{2}} \frac{ie^{i\kappa(\mathbf{k})r_M}}{\kappa(\mathbf{k})} \mathcal{F}[f](\mathbf{h}(\mathbf{k})) \quad \text{for all } \mathbf{k} = (k_1, k_2) \in \mathcal{B}_{k_0}^2, \quad (2.6)$$

where we define as abbreviations the functions

$$\begin{aligned} \mathbf{h}: \mathcal{B}_{k_0}^2 &\rightarrow \mathbb{R}^3, \\ \mathbf{k} \mapsto \mathbf{h}(\mathbf{k}) &:= \begin{pmatrix} \mathbf{k} \\ \kappa(\mathbf{k}) - k_0 \end{pmatrix}, \end{aligned} \quad (2.7)$$

and

$$\begin{aligned} \kappa: \mathcal{B}_{k_0}^2 &\rightarrow [0, k_0], \\ \mathbf{k} \mapsto \kappa(\mathbf{k}) &:= \sqrt{k_0^2 - \|\mathbf{k}\|^2}. \end{aligned} \quad (2.8)$$

Hereby, we use for the d -dimensional Fourier transform $\mathcal{F}^{(d)}: L^2(\mathbb{R}^d \rightarrow \mathbb{C}) \rightarrow L^2(\mathbb{R}^d \rightarrow \mathbb{C})$ the convention for which we have for every continuous function $g: \mathbb{R}^d \rightarrow \mathbb{C}$ with compact support

$$\mathcal{F}^{(d)}[g](\mathbf{y}) := (2\pi)^{-d/2} \int_{\mathbb{R}^d} g(\mathbf{x}) e^{-i\langle \mathbf{x}, \mathbf{y} \rangle} \, d\mathbf{x}, \quad \mathbf{y} \in \mathbb{R}^d. \quad (2.9)$$

Since we will mostly need the three-dimensional Fourier transform, we abbreviate $\mathcal{F} := \mathcal{F}^{(3)}$. Moreover, we define the partial Fourier transform $\mathcal{F}_{1,2}: L^2(\mathbb{R}^3 \rightarrow \mathbb{C}) \rightarrow L^2(\mathbb{R}^3 \rightarrow \mathbb{C})$ in the first two components as the continuous extension of

$$\mathcal{F}_{1,2}[g](k_1, k_2, x_3) := (2\pi)^{-1} \int_{\mathbb{R}^2} g(x_1, x_2, x_3) e^{-i(x_1 k_1 + x_2 k_2)} \, d(x_1, x_2), \quad (k_1, k_2, x_3)^\top \in \mathbb{R}^3, \quad (2.10)$$

for all continuous function $g: \mathbb{R}^3 \rightarrow \mathbb{C}$ with compact support.

2.2 Motion of the object

In our setting, we record diffraction images while exposing the object of interest to an unknown rigid motion

$$\begin{aligned} \Psi: [0, T] \times \mathbb{R}^3 &\rightarrow \mathbb{R}^3, \\ (t, \mathbf{x}) \mapsto \Psi_t(\mathbf{x}) &:= R_t^\top \mathbf{x} + \mathbf{d}_t, \end{aligned} \quad (2.11)$$

which rotates the object by the rotation matrix $R_t^\top \in \text{SO}(3) := \{Q \in \mathbb{R}^{3 \times 3} : Q^\top Q = I, \det Q = 1\}$, and translates it by the vector $\mathbf{d}_t \in \mathbb{R}^3$. Hereby, we consider the object at time $t = 0$ as the reference object and set correspondingly Ψ_0 to be the identity map, that is, $R_0 := I$ and $\mathbf{d}_0 := \mathbf{0}$.

The scattering potential of the object that is exposed to this rigid motion Ψ is then described by the function $t \mapsto f \circ \Psi_t^{-1}$, where the inverse function Ψ_t^{-1} is explicitly given by

$$\Psi_t^{-1}(\mathbf{y}) = R_t(\mathbf{y} - \mathbf{d}_t). \quad (2.12)$$

The diffraction images are now obtained by continuously illuminating the moving object with the incident wave u^{inc} given by (2.1), and recording the resulting scattered wave (which we will approximate by its Born approximation) on the detector surface $\{\mathbf{x} \in \mathbb{R}^3 : x_3 = r_M\}$. We denote by u_t , $t \in [0, T]$, the Born approximation of the wave scattered in the presence of the transformed scattering potential $f \circ \Psi_t^{-1}$, which satisfies the system (2.5) with f replaced by $f \circ \Psi_t^{-1}$, that is, the differential equation

$$\Delta u_t + k_0^2 u_t = -(f \circ \Psi_t^{-1}) u^{\text{inc}}$$

together with radiation condition

$$\lim_{r \rightarrow \infty} \max_{\|\mathbf{x}\|=r} \|\mathbf{x}\| \left| \left\langle \nabla u_t(\mathbf{x}), \frac{\mathbf{x}}{\|\mathbf{x}\|} \right\rangle - ik_0 u_t(\mathbf{x}) \right| = 0.$$

The recorded measurement data is then given by the function

$$\begin{aligned} m: [0, T] \times \mathbb{R}^2 &\rightarrow \mathbb{R}, \\ (t, x_1, x_2) &\mapsto m_t(x_1, x_2) := u_t(x_1, x_2, r_M). \end{aligned} \quad (2.13)$$

Switching to the Fourier domain with respect to x_1 and x_2 , we find with (2.6) for $\mathbf{k} \in \mathcal{B}_{k_0}^2$

$$\begin{aligned} \mathcal{F}^{(2)}[m_t](\mathbf{k}) &= \sqrt{\frac{\pi}{2}} \frac{ie^{i\kappa(\mathbf{k})r_M}}{\kappa(\mathbf{k})} \mathcal{F}[f \circ \Psi_t^{-1}](\mathbf{h}(\mathbf{k})) \\ &= \sqrt{\frac{\pi}{2}} \frac{ie^{i\kappa(\mathbf{k})r_M}}{\kappa(\mathbf{k})} (2\pi)^{-\frac{3}{2}} \int_{\mathbb{R}^3} f(R_t(\mathbf{y} - \mathbf{d}_t)) e^{-i\langle \mathbf{y}, \mathbf{h}(\mathbf{k}) \rangle} d\mathbf{y} \\ &= \sqrt{\frac{\pi}{2}} \frac{ie^{i\kappa(\mathbf{k})r_M}}{\kappa(\mathbf{k})} (2\pi)^{-\frac{3}{2}} \int_{\mathbb{R}^3} f(\tilde{\mathbf{y}}) e^{-i\langle R_t^\top \tilde{\mathbf{y}} + \mathbf{d}_t, \mathbf{h}(\mathbf{k}) \rangle} d\tilde{\mathbf{y}} \end{aligned}$$

and hence the explicit relation

$$\mathcal{F}^{(2)}[m_t](\mathbf{k}) = \sqrt{\frac{\pi}{2}} \frac{ie^{i\kappa(\mathbf{k})r_M}}{\kappa(\mathbf{k})} \mathcal{F}[f](R_t \mathbf{h}(\mathbf{k})) e^{-i\langle \mathbf{d}_t, \mathbf{h}(\mathbf{k}) \rangle} \quad (2.14)$$

between the measurement data m_t and the unknown scattering potential f , which depends on the unknown parameters R_t and \mathbf{d}_t describing the motion of the object.

In the following, we will exploit the relation (2.14) to recover these unknown motion parameters: We will first reconstruct the rotation matrix R_t from the absolute values $|\mathcal{F}[m_t]|$ (taking the absolute value removes the dependency on the translations \mathbf{d}_t , which only enter into the Fourier transform as a phase factor). For this, we propose two different approaches: The first one, called the method of common circles, is presented in Section 3. It is in the spirit of the method of common lines for the ray transform. The second one, presented in Section 4, assumes that the rotations R_t depend smoothly on the time t and calculates, inspired by the ideas in [7], the change in the angular velocity during the motion.

We want to stress at this point that the possible reduction of the data to the absolute values $|\mathcal{F}[m_t]|$ for the reconstruction of the rotations is not directly connected to the phaseless optical diffraction measurements, where only the absolute values $|u^{\text{sca}}(x_1, x_2, r_M)|$, $x_1, x_2 \in \mathbb{R}$, of the scattered wave u^{sca} are detected.

Later, in [Section 5](#), we will use the full data $\mathcal{F}[m_t]$ to further reconstruct the translation vectors \mathbf{d}_t .

With the knowledge of these parameters, the relation (2.14) provides us explicitly with all Fourier data of the scattering potential f which enter the data (ignoring the Fourier components $\mathcal{F}^{(2)}[m_t](\mathbf{k})$ of m_t with $\|\mathbf{k}\| \geq k_0$). From this, we can then reconstruct the scattering potential as described in [19], but we will not discuss this problem in the present paper.

3 Common Circle Method

Given measurement data m of the form (2.13), we define the *scaled squared energy* ν of m by

$$\begin{aligned} \nu_t: \mathcal{B}_{k_0}^2 &\rightarrow [0, \infty), \\ \mathbf{k} = (k_1, k_2)^\top &\mapsto \nu_t(\mathbf{k}) := \frac{2}{\pi} \kappa^2(\mathbf{k}) \left| \mathcal{F}^{(2)}[m_t](\mathbf{k}) \right|^2. \end{aligned} \quad (3.1)$$

According to (2.14), this can be expressed in terms of the scattering potential f by

$$\nu_t(\mathbf{k}) = |\mathcal{F}[f](R_t \mathbf{h}(\mathbf{k}))|^2, \quad \mathbf{k} \in \mathcal{B}_{k_0}^2, t \in [0, T], \quad (3.2)$$

which is independent of the translation vectors \mathbf{d}_t .

If we now compare the scaled squared energies ν_s and ν_t for two different times $s, t \in [0, T]$, we observe that they are not completely independent from each other, but they will share (regardless of the unknown scattering potential) the same value $\nu_s(\mathbf{k}_{s,t}) = \nu_t(\mathbf{k}_{t,s})$ at all pairs $(\mathbf{k}_{s,t}, \mathbf{k}_{t,s}) \in \mathcal{B}_{k_0}^2 \times \mathcal{B}_{k_0}^2$ of points fulfilling the condition

$$R_s(\mathbf{h}(\mathbf{k}_{s,t})) = R_t(\mathbf{h}(\mathbf{k}_{t,s})). \quad (3.3)$$

Our method of common circles aims to recover the relative rotation $R_t^\top R_s$ for every pair $(s, t) \in [0, T]^2$ of times with $s \neq t$, by finding all the associated pairs $(\mathbf{k}_{s,t}, \mathbf{k}_{t,s}) \in \mathcal{B}_{k_0}^2 \times \mathcal{B}_{k_0}^2$ of points.

We define the sets

$$\mathcal{H}_t := \left\{ R_t \mathbf{h}(\mathbf{k}) : \mathbf{k} \in \mathcal{B}_{k_0}^2 \right\}, \quad t \in [0, T],$$

which from the definition (2.7) of the function \mathbf{h} can be seen to be the hemispheres with radius k_0 and center $-k_0 R_t \mathbf{e}^3$, i.e.,

$$\mathcal{H}_t = \{ R_t \mathbf{y} \in \partial \mathcal{B}_{k_0}^3(-k_0 \mathbf{e}^3) : y_3 > -k_0 \} = \{ \mathbf{x} \in \partial \mathcal{B}_{k_0}^3(-k_0 R_t \mathbf{e}^3) : \langle \mathbf{x}, R_t \mathbf{e}^3 \rangle > -k_0 \}, \quad (3.4)$$

where we denote by $\partial \mathcal{B}_{k_0}^3(\mathbf{z}) := \{ \mathbf{y} \in \mathbb{R}^3 : \|\mathbf{y} - \mathbf{z}\| = k_0 \}$ the sphere with center $\mathbf{z} \in \mathbb{R}^3$. If we measured the scattered wave not only behind the object but also in front of the object, i.e., performing both transmission and reflection imaging; then we would have data on the whole sphere $\partial \mathcal{B}_{k_0}^3(-k_0 R_t \mathbf{e}^3)$ instead of only on the hemisphere \mathcal{H}_t , cf. [19].

For fixed $s, t \in [0, T]$ with $s \neq t$, we then consider the intersection $\mathcal{H}_s \cap \mathcal{H}_t$ of such hemispheres, which gives us an arc of a circle in the bisecting plane of the two centers $-k_0 R_s \mathbf{e}^3$ and $-k_0 R_t \mathbf{e}^3$ of the hemispheres. Therefore, we call the resulting technique the ‘‘common circle’’ method, see [Figure 3](#) for an illustration of the intersection.

3.1 Parameterization of the Common Circles

To derive the curves along which the scaled squared energies ν_s and ν_t coincide, we first parametrize the circular arc which we obtain by intersecting the two hemispheres \mathcal{H}_s and \mathcal{H}_t .

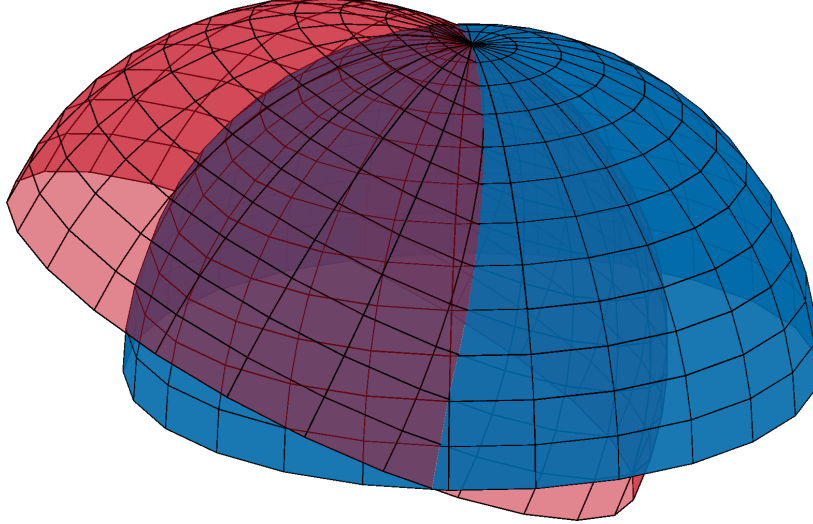


Figure 3: Illustration of the common circles. Two hemispheres \mathcal{H}_0 and \mathcal{H}_t intersect in a common circle arc. The north pole of the hemispheres is at $\mathbf{0}$.

Lemma 3.1 *Let $s, t \in [0, T]$ be such that $R_s \mathbf{e}^3 \neq \pm R_t \mathbf{e}^3$. Then, we can parametrize the intersection in the form $\mathcal{H}_s \cap \mathcal{H}_t = \{\boldsymbol{\sigma}_{s,t}(\beta) : \beta \in J_{s,t}\}$ with the curve*

$$\begin{aligned} \boldsymbol{\sigma}_{s,t}: J_{s,t} &\rightarrow \mathbb{R}^3, \\ \beta &\mapsto \boldsymbol{\sigma}_{s,t}(\beta) := a_{s,t}(\cos(\beta) - 1)\mathbf{v}_{s,t}^1 + a_{s,t} \sin(\beta)\mathbf{v}_{s,t}^2, \end{aligned} \quad (3.5)$$

where we used the positively oriented, orthonormal basis

$$\mathbf{v}_{s,t}^1 := \frac{R_s \mathbf{e}^3 + R_t \mathbf{e}^3}{\|R_s \mathbf{e}^3 + R_t \mathbf{e}^3\|}, \quad \mathbf{v}_{s,t}^2 := \frac{(R_s \mathbf{e}^3) \times (R_t \mathbf{e}^3)}{\|(R_s \mathbf{e}^3) \times (R_t \mathbf{e}^3)\|}, \quad \mathbf{v}_{s,t}^3 := \frac{R_s \mathbf{e}^3 - R_t \mathbf{e}^3}{\|R_s \mathbf{e}^3 - R_t \mathbf{e}^3\|}, \quad (3.6)$$

the radius $a_{s,t} := \frac{k_0}{2} \|R_s \mathbf{e}^3 + R_t \mathbf{e}^3\|$ and the interval

$$J_{s,t} := \begin{cases} (-\pi, \pi] & \text{if } \langle R_s \mathbf{e}^3, R_t \mathbf{e}^3 \rangle \leq 0, \\ (-\beta_{s,t}, \beta_{s,t}) & \text{if } \langle R_s \mathbf{e}^3, R_t \mathbf{e}^3 \rangle > 0 \end{cases} \quad \text{with } \beta_{s,t} := \arccos \left(\frac{\langle R_s \mathbf{e}^3, R_t \mathbf{e}^3 \rangle - 1}{\langle R_s \mathbf{e}^3, R_t \mathbf{e}^3 \rangle + 1} \right). \quad (3.7)$$

Proof: By (3.4), a point $\mathbf{x} \in \mathbb{R}^3$ is in the intersection $\mathcal{H}_s \cap \mathcal{H}_t$ if and only if it fulfills the equations

$$\|\mathbf{x} + k_0 R_s \mathbf{e}^3\|^2 = k_0^2 \quad \text{and} \quad \|\mathbf{x} + k_0 R_t \mathbf{e}^3\|^2 = k_0^2 \quad (3.8)$$

and the two inequalities

$$\langle \mathbf{x}, R_s \mathbf{e}^3 \rangle > -k_0 \quad \text{and} \quad \langle \mathbf{x}, R_t \mathbf{e}^3 \rangle > -k_0. \quad (3.9)$$

Taking their sum and their difference, the two equations (3.8) are seen to be equivalent to

$$\left\| \mathbf{x} + \frac{k_0}{2} (R_s \mathbf{e}^3 + R_t \mathbf{e}^3) \right\|^2 = \frac{k_0^2}{4} \|R_s \mathbf{e}^3 + R_t \mathbf{e}^3\|^2 \quad \text{and} \quad \langle \mathbf{x}, R_s \mathbf{e}^3 - R_t \mathbf{e}^3 \rangle = 0,$$

meaning that \mathbf{x} is on a circle with radius $a_{s,t}$ around the point $-a_{s,t} \mathbf{v}_{s,t}^1$ in the subspace $\mathcal{V}_{s,t}$ spanned by the vectors $\mathbf{v}_{s,t}^1$ and $\mathbf{v}_{s,t}^2$, so that we can write

$$\mathbf{x} = a_{s,t}(\cos(\beta) - 1)\mathbf{v}_{s,t}^1 + a_{s,t} \sin(\beta)\mathbf{v}_{s,t}^2 \quad \text{for some } \beta \in (-\pi, \pi].$$

For such a point \mathbf{x} , the two inequalities (3.9) are equivalent and reduce to the condition

$$\frac{k_0}{2} (\cos(\beta) - 1)(1 + \langle R_s \mathbf{e}^3, R_t \mathbf{e}^3 \rangle) > -k_0, \quad \text{that is, } \cos(\beta) > \frac{\langle R_s \mathbf{e}^3, R_t \mathbf{e}^3 \rangle - 1}{\langle R_s \mathbf{e}^3, R_t \mathbf{e}^3 \rangle + 1}$$

for the variable β . □

To see at which positions in ν_s and ν_t the shared data points from $\mathcal{H}_s \cap \mathcal{H}_t$ are, we write the intersection via the parametrization $R_s \mathbf{h}$ and $R_t \mathbf{h}$, respectively, which is illustrated in Figure 4. We denote the orthogonal projection to the first two components by

$$\begin{aligned} P: \mathbb{R}^3 &\rightarrow \mathbb{R}^2, \\ (x_1, x_2, x_3)^\top &\mapsto P(x_1, x_2, x_3)^\top := (x_1, x_2)^\top. \end{aligned} \quad (3.10)$$

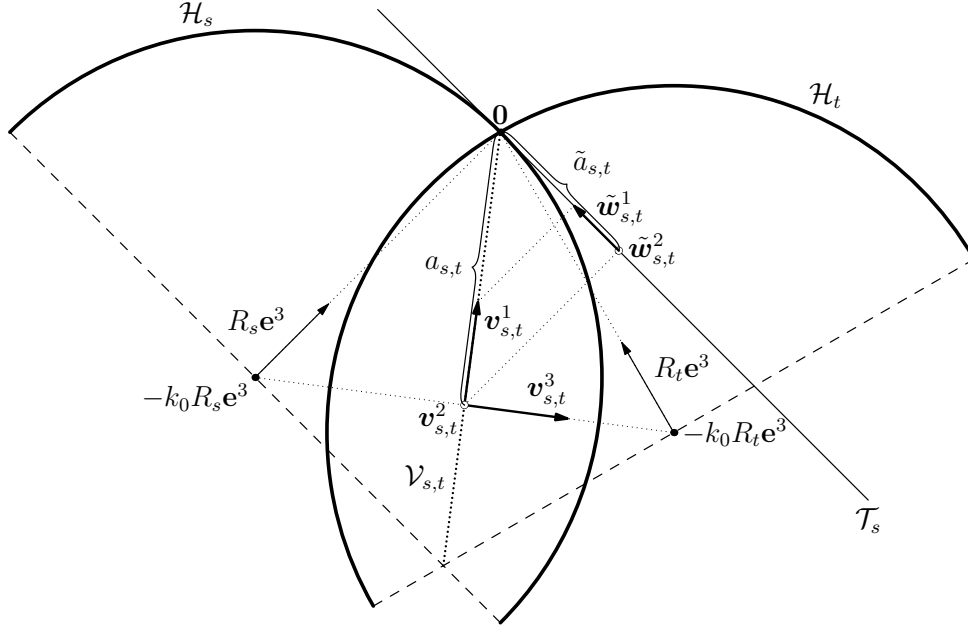


Figure 4: The intersection of two hemispheres \mathcal{H}_s and \mathcal{H}_t in the plane through the centers of the hemispheres and the origin. The circular arc $\mathcal{H}_s \cap \mathcal{H}_t$ lies in the plane $\mathcal{V}_{s,t} = \{\mathbf{x} \in \mathbb{R}^3 : \langle \mathbf{x}, (R_s - R_t)\mathbf{e}^3 \rangle = 0\}$ perpendicular to the line between the centers. This plane is spanned by the first two vectors of the basis $(\mathbf{v}_{s,t}^j)_{j=1}^3$ used in Lemma 3.1 to describe the arc. The basis $(\mathbf{w}_{s,t}^j)_{j=1}^2$ of \mathbb{R}^2 introduced in Lemma 3.2 is illustrated by the orthogonal projection $(\tilde{\mathbf{w}}_{s,t}^j)_{j=1}^2$ of $(\mathbf{v}_{s,t}^j)_{j=1}^2$ to the tangent plane \mathcal{T}_s of \mathcal{H}_s at $\mathbf{0}$. They are explicitly related by $\mathbf{w}_{s,t}^j = P(R_s^\top \tilde{\mathbf{w}}_{s,t}^j)$.

Lemma 3.2 *Let $s, t \in [0, T]$ be such that $R_s \mathbf{e}^3 \neq \pm R_t \mathbf{e}^3$ and let $\sigma_{s,t}$ be defined as in Lemma 3.1. Then, we have*

$$\sigma_{s,t}(\beta) = R_s \mathbf{h}(\gamma_{s,t}(\beta)) \quad \text{for all } \beta \in J_{s,t} \quad (3.11)$$

with the elliptic arc

$$\begin{aligned} \gamma_{s,t}: J_{s,t} &\rightarrow \mathcal{B}_{k_0}^2, \\ \beta &\mapsto \gamma_{s,t}(\beta) := \tilde{a}_{s,t}(\cos(\beta) - 1)\mathbf{w}_{s,t}^1 + a_{s,t} \sin(\beta)\mathbf{w}_{s,t}^2, \end{aligned} \quad (3.12)$$

which has the semi-axes $\tilde{a}_{s,t} := \frac{k_0}{2} \|P(R_s^\top R_t \mathbf{e}^3)\|$ and $a_{s,t}$, which is defined as in Lemma 3.1 by $a_{s,t} = \frac{k_0}{2} \|R_s \mathbf{e}^3 + R_t \mathbf{e}^3\|$, and the directions of the axes are given by

$$\mathbf{w}_{s,t}^1 = \frac{P(R_s^\top R_t \mathbf{e}^3)}{\|P(R_s^\top R_t \mathbf{e}^3)\|} \quad \text{and} \quad \mathbf{w}_{s,t}^2 = \frac{P(\mathbf{e}^3 \times (R_s^\top R_t \mathbf{e}^3))}{\|P(\mathbf{e}^3 \times (R_s^\top R_t \mathbf{e}^3))\|}. \quad (3.13)$$

Proof: Since $R_s \mathbf{h}$ is a parametrization of \mathcal{H}_s and \mathbf{h} restricted to its first two components is just the identity, we can solve the relation $R_s \mathbf{h}(\mathbf{k}) = \mathbf{x}$ for every $\mathbf{x} \in \mathcal{H}_s$ by orthogonally projecting $R_s^\top \mathbf{x}$ onto its first two components

$$\mathbf{k} = P(R_s^\top \mathbf{x}).$$

Therefore we find directly from the representation (3.5) of $\mathcal{H}_s \cap \mathcal{H}_t$ that

$$\gamma_{s,t}(\beta) = a_{s,t}(\cos(\beta) - 1)P(R_s^\top \mathbf{v}_{s,t}^1) + a_{s,t} \sin(\beta)P(R_s^\top \mathbf{v}_{s,t}^2). \quad (3.14)$$

Further we get for the projections of the basis vectors

$$\begin{aligned} P(R_s^\top \mathbf{v}_{s,t}^1) &= \frac{P(\mathbf{e}^3 + R_s^\top R_t \mathbf{e}^3)}{\|R_s \mathbf{e}^3 + R_t \mathbf{e}^3\|} = \frac{\tilde{a}_{s,t}}{a_{s,t}} \mathbf{w}_{s,t}^1 \quad \text{and} \\ P(R_s^\top \mathbf{v}_{s,t}^2) &= \frac{P(\mathbf{e}^3 \times (R_s^\top R_t \mathbf{e}^3))}{\|(R_s \mathbf{e}^3) \times (R_t \mathbf{e}^3)\|} = \mathbf{w}_{s,t}^2, \end{aligned} \quad (3.15)$$

so that the equation (3.14) for $\gamma_{s,t}$ becomes (3.12). \square

By interchanging s and t , we see that the curves $\gamma_{s,t}$ and the reversed curve $\gamma_{t,s}^-: J_{t,s} \rightarrow \mathcal{B}_{k_0}^2$, defined by $\gamma_{t,s}^-(\beta) := \gamma_{t,s}(-\beta)$, give us an explicit parametrization of the points $\mathbf{k}_{s,t}$ and $\mathbf{k}_{t,s}$ in the desired relation (3.3).

Proposition 3.3 *Let $s, t \in [0, T]$ be such that $R_s \mathbf{e}^3 \neq \pm R_t \mathbf{e}^3$. Then the elliptic arcs $\gamma_{s,t}$ and $\gamma_{t,s}$ defined by (3.12) fulfill the relations*

$$R_s \mathbf{h}(\gamma_{s,t}(\beta)) = R_t \mathbf{h}(\gamma_{t,s}(-\beta)) \quad \text{and therefore} \quad (3.16)$$

$$\nu_s(\gamma_{s,t}(\beta)) = \nu_t(\gamma_{t,s}(-\beta)) \quad \text{for all } \beta \in J_{s,t}. \quad (3.17)$$

Proof: We remark that the circular arcs $\sigma_{s,t}$ and $\sigma_{t,s}$ given by (3.5) fulfill by definition $\sigma_{s,t}(\beta) = \sigma_{t,s}(-\beta)$ for all $\beta \in J_{s,t} = J_{t,s}$. Therefore, the equation (3.11) implies

$$R_s \mathbf{h}(\gamma_{s,t}(\beta)) = \sigma_{s,t}(\beta) = \sigma_{t,s}(-\beta) = R_t \mathbf{h}(\gamma_{t,s}(-\beta)) \quad \text{for all } \beta \in J_{s,t}$$

And according to the expression (3.2) for ν , this directly yields $\nu_s(\gamma_{s,t}(\beta)) = \nu_t(\gamma_{t,s}(-\beta))$ for all $\beta \in J_{s,t}$. \square

If we are able to detect from (3.17) the two elliptic arcs, $\gamma_{s,t}$ in the image ν_s and $\gamma_{t,s}$ in the image ν_t , this gives us access to the directions $\mathbf{w}_{s,t}^1, \mathbf{w}_{t,s}^1 \in \mathbb{S}^1$ and the lengths $a_{s,t} = a_{t,s}$ of the semi-axes through the origin of the arcs as well as the lengths $\tilde{a}_{s,t} = \frac{k_0}{2} \sqrt{(R_s^\top R_t)_{13}^2 + (R_s^\top R_t)_{23}^2} = \frac{k_0}{2} \sqrt{1 - (R_s^\top R_t)_{33}^2} = \tilde{a}_{t,s}$ of the two other semi-axes. To make it explicit that this information is sufficient to determine the rotation matrix $R_s^\top R_t = (R_t^\top R_s)^\top$, we will parametrize the matrix with *Euler angles*.

That is, we make use of the fact, that every rotation matrix $R \in \text{SO}(3)$ can be written (in the z - y - z convention) in the form

$$R = R^{(3)}(\varphi)R^{(2)}(\theta)R^{(3)}(\psi)$$

with the Euler angles $\varphi, \psi \in \mathbb{R}/(2\pi\mathbb{Z})$ and $\theta \in [0, \pi]$, where $R^{(2)}$ and $R^{(3)}$ denote the rotation matrices

$$R^{(2)}(\alpha) := \begin{pmatrix} \cos(\alpha) & 0 & \sin(\alpha) \\ 0 & 1 & 0 \\ -\sin(\alpha) & 0 & \cos(\alpha) \end{pmatrix} \quad \text{and} \quad R^{(3)}(\alpha) := \begin{pmatrix} \cos(\alpha) & -\sin(\alpha) & 0 \\ \sin(\alpha) & \cos(\alpha) & 0 \\ 0 & 0 & 1 \end{pmatrix}, \quad \alpha \in \mathbb{R},$$

around the \mathbf{e}^2 and \mathbf{e}^3 axis, respectively. The Euler angles are uniquely defined if we set $\psi = 0$ for $\theta \in \{0, \pi\}$.

Lemma 3.4 Let $s, t \in [0, T]$ be such that $R_s \mathbf{e}^3 \neq \pm R_t \mathbf{e}^3$ and $(\varphi, \theta, \psi) \in (\mathbb{R}/(2\pi\mathbb{Z})) \times [0, \pi] \times (\mathbb{R}/(2\pi\mathbb{Z}))$ be the Euler angles of the rotation $R_s^\top R_t$:

$$R_s^\top R_t = R^{(3)}(\varphi)R^{(2)}(\theta)R^{(3)}(\psi). \quad (3.18)$$

Then the elliptic arc $\gamma_{s,t}$ from (3.12) is given in terms of the Euler angles by

$$\gamma_{s,t}(\beta) = \frac{k_0}{2} \sin(\theta)(\cos(\beta) - 1) \begin{pmatrix} \cos(\varphi) \\ \sin(\varphi) \end{pmatrix} + k_0 \cos(\frac{\theta}{2}) \sin(\beta) \begin{pmatrix} -\sin(\varphi) \\ \cos(\varphi) \end{pmatrix}, \quad \beta \in J_{s,t}. \quad (3.19)$$

Proof: We have that

$$R_s^\top R_t \mathbf{e}^3 = R^{(3)}(\varphi)R^{(2)}(\theta)R^{(3)}(\psi)\mathbf{e}^3 = R^{(3)}(\varphi)R^{(2)}(\theta)\mathbf{e}^3 = \begin{pmatrix} \cos(\varphi) \sin(\theta) \\ \sin(\varphi) \sin(\theta) \\ \cos(\theta) \end{pmatrix}.$$

Plugging this into $\gamma_{s,t}$ from (3.12), we find for the lengths of the semi-axes

$$\begin{aligned} \tilde{a}_{s,t} &= \frac{k_0}{2} \left\| P(R_s^\top R_t \mathbf{e}^3) \right\| = \frac{k_0}{2} \sin(\theta) \quad \text{and} \\ a_{s,t} &= \frac{k_0}{2} \left\| R_s \mathbf{e}^3 + R_t \mathbf{e}^3 \right\| = \frac{k_0}{2} \left\| \mathbf{e}^3 + R_s^\top R_t \mathbf{e}^3 \right\| = \frac{k_0}{2} \sqrt{2 + 2 \cos(\theta)} = k_0 \cos(\frac{\theta}{2}); \end{aligned}$$

and for the directions of the semi-axes $\mathbf{w}_{s,t}^1 = \begin{pmatrix} \cos(\varphi) \\ \sin(\varphi) \end{pmatrix}$ and $\mathbf{w}_{s,t}^2 = \begin{pmatrix} -\sin(\varphi) \\ \cos(\varphi) \end{pmatrix}$. \square

If the function values of $\mathcal{F}[f]$ would always take different values at different points, the only matching points in ν_s and ν_t would be (as seen in (3.16)) those on the elliptic arcs $\gamma_{s,t}$ and $\gamma_{t,s}$. However, since our scattering potential f is real-valued, its Fourier transform has the symmetry

$$\mathcal{F}[f](-\mathbf{x}) = \overline{\mathcal{F}[f](\mathbf{x})} \quad \text{for all } \mathbf{x} \in \mathbb{R}^3. \quad (3.20)$$

Thus, we have to look besides the condition (3.3) also for points $\check{\mathbf{k}}_{s,t}, \check{\mathbf{k}}_{t,s} \in \mathcal{B}_{k_0}^2$ with

$$R_s(\mathbf{h}(\check{\mathbf{k}}_{s,t})) = -R_t(\mathbf{h}(\check{\mathbf{k}}_{t,s})) \quad (3.21)$$

as they would fulfill $\nu_s(\check{\mathbf{k}}_{s,t}) = \nu_t(\check{\mathbf{k}}_{t,s})$, too. The points (3.21) are in the intersection of \mathcal{H}_s and the reflected hemisphere $-\mathcal{H}_t = \{-\mathbf{x} : \mathbf{x} \in \mathcal{H}_t\}$. We derive the curves describing these points in the same way as we obtained the elliptic arcs $\gamma_{s,t}$ by parametrizing $\mathcal{H}_s \cap (-\mathcal{H}_t)$ as follows.

Lemma 3.5 Let $s, t \in [0, T]$ be such that $R_s \mathbf{e}^3 \neq R_t \mathbf{e}^3$.

(i) Using the basis $(\mathbf{v}_{s,t}^j)_{j=1}^3$ introduced in (3.6), the intersection of \mathcal{H}_s and $-\mathcal{H}_t$ can be parametrized as $\mathcal{H}_s \cap (-\mathcal{H}_t) = \{\check{\boldsymbol{\sigma}}_{s,t}(\beta) : \beta \in \check{J}_{s,t}\}$ with

$$\begin{aligned} \check{\boldsymbol{\sigma}}_{s,t}: \check{J}_{s,t} &\rightarrow \mathbb{R}^3, \\ \beta &\mapsto \check{\boldsymbol{\sigma}}_{s,t}(\beta) := \check{a}_{s,t}(\cos(\beta) - 1)\mathbf{v}_{s,t}^3 - \check{a}_{s,t} \sin(\beta)\mathbf{v}_{s,t}^2, \end{aligned} \quad (3.22)$$

where $\check{a}_{s,t} := \frac{k_0}{2} \|R_s \mathbf{e}^3 - R_t \mathbf{e}^3\|$ and

$$\begin{aligned} \check{J}_{s,t} &:= \begin{cases} (-\pi, \pi] & \text{if } \langle R_s \mathbf{e}^3, R_t \mathbf{e}^3 \rangle \geq 0, \\ (-\check{\beta}_{s,t}, \check{\beta}_{s,t}) & \text{if } \langle R_s \mathbf{e}^3, R_t \mathbf{e}^3 \rangle < 0 \end{cases} \quad \text{with} \\ \check{\beta}_{s,t} &:= \arccos \left(\frac{\langle R_s \mathbf{e}^3, R_t \mathbf{e}^3 \rangle + 1}{\langle R_s \mathbf{e}^3, R_t \mathbf{e}^3 \rangle - 1} \right). \end{aligned} \quad (3.23)$$

(ii) We have

$$\check{\sigma}_{s,t}(\beta) = R_s \mathbf{h}(\check{\gamma}_{s,t}(\beta)) \quad \text{for all } \beta \in \check{J}_{s,t} \quad (3.24)$$

with the elliptic arc $\check{\gamma}_{s,t}$ being given in the basis $(\mathbf{w}_{s,t}^j)_{j=1}^2$ from (3.13) with the semi-axis $\check{a}_{s,t} = \frac{k_0}{2} \left\| P(R_s^\top R_t \mathbf{e}^3) \right\|$ from Lemma 3.2 by

$$\begin{aligned} \check{\gamma}_{s,t}: \check{J}_{s,t} &\rightarrow \mathcal{B}_{k_0}^2, \\ \beta &\mapsto \check{\gamma}_{s,t}(\beta) := -\check{a}_{s,t}(\cos(\beta) - 1) \mathbf{w}_{s,t}^1 - \check{a}_{s,t} \sin(\beta) \mathbf{w}_{s,t}^2. \end{aligned} \quad (3.25)$$

(iii) With $(\varphi, \theta, \psi) \in (\mathbb{R}/(2\pi\mathbb{Z})) \times [0, \pi] \times (\mathbb{R}/(2\pi\mathbb{Z}))$ denoting the Euler angles of the rotation $R_s^\top R_t$: $R_s^\top R_t = R^{(3)}(\varphi)R^{(2)}(\theta)R^{(3)}(\psi)$; the elliptic arc $\check{\gamma}_{s,t}$ has the form

$$\check{\gamma}_{s,t}(\beta) = -\frac{k_0}{2} \sin(\theta)(\cos(\beta) - 1) \begin{pmatrix} \cos(\varphi) \\ \sin(\varphi) \end{pmatrix} - k_0 \sin(\frac{\theta}{2}) \sin(\beta) \begin{pmatrix} -\sin(\varphi) \\ \cos(\varphi) \end{pmatrix}. \quad (3.26)$$

Proof: The proof goes along the same lines as Lemma 3.1, Lemma 3.2, and Lemma 3.4.

- (i) By replacing $R_t \mathbf{e}^3$ by $-R_t \mathbf{e}^3$ in Lemma 3.1, we directly get the parametrization $\check{\sigma}_{s,t}$ of $\mathcal{H}_s \cap (-\mathcal{H}_t)$ in the form of (3.22).
- (ii) Proceeding as in Lemma 3.2, we find the curve $\check{\gamma}_{s,t}$ by

$$\check{\gamma}_{s,t}(\beta) = P(R_s^\top \check{\sigma}_{s,t}(\beta)) = \check{a}_{s,t}(\cos(\beta) - 1) P(R_s^\top \mathbf{v}_{s,t}^3) - \check{a}_{s,t} \sin(\beta) P(R_s^\top \mathbf{v}_{s,t}^2).$$

With

$$P(R_s^\top \mathbf{v}_{s,t}^3) = \frac{P(\mathbf{e}^3 - R_s^\top R_t \mathbf{e}^3)}{\|R_s \mathbf{e}^3 - R_t \mathbf{e}^3\|} = -\frac{k_0 P(R_s^\top R_t \mathbf{e}^3)}{2 \check{a}_{s,t}} = -\frac{\check{a}_{s,t}}{\check{a}_{s,t}} \mathbf{w}_{s,t}^1, \quad (3.27)$$

this yields the equation (3.25) for $\check{\gamma}_{s,t}$.

- (iii) Taking finally the expressions of $\check{a}_{s,t}$, $\mathbf{w}_{s,t}^1$, and $\mathbf{w}_{s,t}^2$ in terms of the Euler angles of $R_s^\top R_t$ from the proof of Lemma 3.4, we obtain with

$$\check{a}_{s,t} := \frac{k_0}{2} \left\| \mathbf{e}^3 - R_s^\top R_t \mathbf{e}^3 \right\| = \frac{k_0}{2} \sqrt{2 - 2 \cos(\theta)} = k_0 \sin(\frac{\theta}{2})$$

the identity in (3.26). □

As in Proposition 3.3, this gives us the equality of the values of ν_s and ν_t along the elliptic arcs $\check{\gamma}_{s,t}$ and $\check{\gamma}_{t,s}$.

Proposition 3.6 *Let $s, t \in [0, T]$ be such that $R_s \mathbf{e}^3 \neq \pm R_t \mathbf{e}^3$. Then the elliptic arcs $\check{\gamma}_{s,t}$ and $\check{\gamma}_{t,s}$ defined by (3.25) fulfill the relations*

$$R_s \mathbf{h}(\check{\gamma}_{s,t}(\beta)) = -R_t \mathbf{h}(\check{\gamma}_{t,s}(\beta)) \quad \text{and therefore} \quad (3.28)$$

$$\nu_s(\check{\gamma}_{s,t}(\beta)) = \nu_t(\check{\gamma}_{t,s}(\beta)) \quad \text{for all } \beta \in \check{J}_{s,t}. \quad (3.29)$$

Proof: We remark that the circular arcs $\check{\sigma}_{s,t}$ and $\check{\sigma}_{t,s}$ given by (3.22) fulfill by definition $\check{\sigma}_{s,t}(\beta) = -\check{\sigma}_{t,s}(\beta)$ for all $\beta \in \check{J}_{s,t} = \check{J}_{t,s}$. Therefore, the equation (3.24) implies

$$R_s \mathbf{h}(\check{\gamma}_{s,t}(\beta)) = \check{\sigma}_{s,t}(\beta) = -\check{\sigma}_{t,s}(\beta) = -R_t \mathbf{h}(\check{\gamma}_{t,s}(\beta)) \quad \text{for all } \beta \in \check{J}_{s,t}.$$

And using the symmetry (3.20) in the expression (3.2) for ν , this directly yields $\nu_s(\check{\gamma}_{s,t}(\beta)) = \nu_t(\check{\gamma}_{t,s}(\beta))$ for all $\beta \in \check{J}_{s,t}$. □

We summarize the resulting reconstruction method, illustrated in [Figure 5](#), in the following [Theorem 3.9](#). But, first, we want to mention that the special cases $R_s \mathbf{e}^3 = \pm R_t \mathbf{e}^3$ can (in the generic case) easily be detected.

Lemma 3.7 *Let $s, t \in [0, T]$ be such that $R_s \mathbf{e}^3 = R_t \mathbf{e}^3$. Then we have the representation $R_s^\top R_t = R^{(3)}(\psi)$ for some $\psi \in \mathbb{R}/(2\pi\mathbb{Z})$ in Euler angles and*

$$\nu_s(\hat{R}^{(3)}(\psi)\mathbf{k}) = \nu_t(\mathbf{k}) \quad \text{for all } \mathbf{k} \in \mathcal{B}_{k_0}^2, \quad \hat{R}^{(3)}(\psi) := \begin{pmatrix} \cos(\psi) & -\sin(\psi) \\ \sin(\psi) & \cos(\psi) \end{pmatrix}. \quad (3.30)$$

Proof: Since $R_s^\top R_t \mathbf{e}^3 = \mathbf{e}^3$, the rotation $R_s^\top R_t$ has the rotation axis $\mathbb{R}\mathbf{e}^3$ and is therefore of the form $R_s^\top R_t = R^{(3)}(\psi)$ for some $\psi \in \mathbb{R}/(2\pi\mathbb{Z})$. Then, we see from the definition (2.7) of the parametrization \mathbf{h} that we have for all $\mathbf{k} \in \mathcal{B}_{k_0}^2$

$$R_s^\top R_t \mathbf{h}(\mathbf{k}) = R^{(3)}(\psi) \mathbf{h}(\mathbf{k}) = \mathbf{h}(\hat{R}^{(3)}(\psi)\mathbf{k}) \quad (3.31)$$

and therefore, according to (3.2),

$$\nu_s(\hat{R}^{(3)}(\psi)\mathbf{k}) = \left| \mathcal{F}[f](R_s \mathbf{h}(\hat{R}^{(3)}(\psi)\mathbf{k})) \right|^2 = \left| \mathcal{F}[f](R_t \mathbf{h}(\mathbf{k})) \right|^2 = \nu_t(\mathbf{k}). \quad \square$$

Because of the symmetry (3.20), we find also in the case $R_s \mathbf{e}^3 = -R_t \mathbf{e}^3$, where we have $\mathcal{H}_s \cap \mathcal{H}_t = \{\mathbf{0}\}$, such an invariance between ν_s and ν_t as follows.

Lemma 3.8 *Let $s, t \in [0, T]$ be such that $R_s \mathbf{e}^3 = -R_t \mathbf{e}^3$. Then we have the representation $R_s^\top R_t = R^{(2)}(\pi)R^{(3)}(\psi)$ for some $\psi \in \mathbb{R}/(2\pi\mathbb{Z})$ in Euler angles and, with $\hat{R}^{(3)}$ as in (3.30),*

$$\nu_s(S\hat{R}^{(3)}(\psi)\mathbf{k}) = \nu_t(\mathbf{k}) \quad \text{for all } \mathbf{k} \in \mathcal{B}_{k_0}^2, \quad S := \begin{pmatrix} 1 & 0 \\ 0 & -1 \end{pmatrix}. \quad (3.32)$$

Proof: Since $R^{(2)}(\pi)R_s^\top R_t \mathbf{e}^3 = -R^{(2)}(\pi)\mathbf{e}^3 = \mathbf{e}^3$, the rotation $R^{(2)}(\pi)R_s^\top R_t$ has the rotation axis $\mathbb{R}\mathbf{e}^3$ and we therefore have $R_s^\top R_t = R^{(2)}(\pi)R^{(3)}(\psi)$ for some $\psi \in \mathbb{R}/(2\pi\mathbb{Z})$. Then, we see from the definition (2.7) of the parametrization \mathbf{h} that we have for all $\mathbf{k} \in \mathcal{B}_{k_0}^2$

$$R_s^\top R_t \mathbf{h}(\mathbf{k}) = R^{(2)}(\pi)R^{(3)}(\psi) \mathbf{h}(\mathbf{k}) = R^{(2)}(\pi) \mathbf{h}(\hat{R}^{(3)}(\psi)\mathbf{k}) = -\mathbf{h}(S\hat{R}^{(3)}(\psi)\mathbf{k}) \quad (3.33)$$

and therefore, according to (3.2) and (3.20),

$$\nu_s(S\hat{R}^{(3)}(\psi)\mathbf{k}) = \left| \mathcal{F}[f](R_s \mathbf{h}(S\hat{R}^{(3)}(\psi)\mathbf{k})) \right|^2 = \left| \mathcal{F}[f](-R_t \mathbf{h}(\mathbf{k})) \right|^2 = \left| \mathcal{F}[f](R_t \mathbf{h}(\mathbf{k})) \right|^2 = \nu_t(\mathbf{k}). \quad \square$$

Consequently, we can exclude these special cases and reconstruct the relative rotations between the remaining pairs of time steps by finding the common elliptic arcs (provided that unique pairs can be found).

Theorem 3.9 *Let $s, t \in [0, T]$ be such that there does not exist a parameter $\alpha \in \mathbb{R}/(2\pi\mathbb{Z})$ with $\nu_s(\hat{R}^{(3)}(\alpha)\mathbf{k}) = \nu_t(\mathbf{k})$ for all $\mathbf{k} \in \mathcal{B}_{k_0}^2$ nor with $\nu_s(S\hat{R}^{(3)}(\alpha)\mathbf{k}) = \nu_t(\mathbf{k})$ for all $\mathbf{k} \in \mathcal{B}_{k_0}^2$. Furthermore, we assume that there uniquely exist two pairs of elliptic arcs $(\gamma_\ell)_{\ell=1}^2$ and $(\check{\gamma}_\ell)_{\ell=1}^2$ of the form*

$$\begin{aligned} \gamma_\ell: J &\rightarrow \mathcal{B}_{k_0}^2, & \gamma_\ell(\beta) &:= \tilde{a}(\cos(\beta) - 1)\mathbf{w}_\ell^1 + a \sin(\beta)\mathbf{w}_\ell^2, & \text{and} \\ \check{\gamma}_\ell: \check{J} &\rightarrow \mathcal{B}_{k_0}^2, & \check{\gamma}_\ell(\beta) &:= -\tilde{a}(\cos(\beta) - 1)\mathbf{w}_\ell^1 - \check{a} \sin(\beta)\mathbf{w}_\ell^2, & \ell \in \{1, 2\}, \end{aligned}$$

for some parameter $a \in (0, k_0)$, $\check{a} := \sqrt{k_0^2 - a^2} \in (0, k_0)$ and $\tilde{a} := \frac{a}{k_0} \sqrt{k_0^2 - a^2} \in (0, \frac{k_0}{2})$, and two positively oriented, orthonormal bases $(\mathbf{w}_1^j)_{j=1}^2$ and $(\mathbf{w}_2^j)_{j=1}^2$ of \mathbb{R}^2 such that

$$\nu_s(\gamma_1(\beta)) = \nu_t(\gamma_2(-\beta)) \quad \text{for all } \beta \in J \quad \text{and} \quad (3.34)$$

$$\nu_s(\check{\gamma}_1(\beta)) = \nu_t(\check{\gamma}_2(\beta)) \quad \text{for all } \beta \in \check{J} \quad (3.35)$$

for some intervals $J, \check{J} \supset [-\frac{\pi}{2}, \frac{\pi}{2}]$. Then we have

$$R_s^\top R_t = R^{(3)}(\arg(\mathbf{w}_1^1)) R^{(2)}(2 \arccos(\frac{a}{k_0})) R^{(3)}(\pi - \arg(\mathbf{w}_2^1)) \quad (3.36)$$

where the argument function $\arg: \mathbb{S}^1 \rightarrow \mathbb{R}/(2\pi\mathbb{Z})$ is defined by $(\cos(\arg(\mathbf{w})), \sin(\arg(\mathbf{w})))^\top = \mathbf{w}$.

Proof: According to Lemma 3.7 and Lemma 3.8, the fact that neither $\nu_s(\hat{R}^{(3)}(\alpha)\mathbf{k}) = \nu_t(\mathbf{k})$ nor $\nu_s(S\hat{R}^{(3)}(\alpha)\mathbf{k}) = \nu_t(\mathbf{k})$ holds for all $\mathbf{k} \in \mathcal{B}_{k_0}^2$ for any choice of parameter $\alpha \in \mathbb{R}/(2\pi\mathbb{Z})$ excludes the cases where $R_s \mathbf{e}^3 = \pm R_t \mathbf{e}^3$ and we can find the elliptic arcs $\gamma_{s,t}$ and $\gamma_{t,s}$ and the dual arcs $\check{\gamma}_{s,t}$ and $\check{\gamma}_{t,s}$ as in Lemma 3.2 and Lemma 3.5.

We parametrize the matrix $R_s^\top R_t$ in Euler angles $(\varphi, \theta, \psi) \in (\mathbb{R}/(2\pi\mathbb{Z})) \times [0, \pi] \times (\mathbb{R}/(2\pi\mathbb{Z}))$ as in (3.18). Then, the representation of the transposed matrix $R_t^\top R_s$ in Euler angles is given by

$$R_t^\top R_s = (R_s^\top R_t)^\top = R^{(3)}(-\psi) R^{(2)}(-\theta) R^{(3)}(-\varphi) = R^{(3)}(\pi - \psi) R^{(2)}(\theta) R^{(3)}(\pi - \varphi), \quad (3.37)$$

where we used the identity $R^{(2)}(-\theta) = R^{(3)}(\pi) R^{(2)}(\theta) R^{(3)}(\pi)$ to shift the angles for $R_t^\top R_s$ into the chosen area of definition.

Thus, we see from (3.19) that the curves $\gamma_{s,t}$ and $\gamma_{t,s}$ are with the parameters

$$a = a_{s,t} = k_0 \cos(\frac{\theta}{2}) \quad \text{and} \quad \tilde{a} = \tilde{a}_{s,t} = \frac{k_0}{2} \sin(\theta) = k_0 \cos(\frac{\theta}{2}) \sin(\frac{\theta}{2}) = \frac{a}{k_0} \sqrt{k_0^2 - a^2} \quad (3.38)$$

and the basis vectors

$$\mathbf{w}_1^1 = \mathbf{w}_{s,t}^1 = \begin{pmatrix} \cos(\varphi) \\ \sin(\varphi) \end{pmatrix} \quad \text{and} \quad \mathbf{w}_2^1 = \mathbf{w}_{t,s}^1 = \begin{pmatrix} \cos(\pi - \psi) \\ \sin(\pi - \psi) \end{pmatrix} \quad (3.39)$$

of the form of γ_1 and γ_2 . Similarly, the dual arcs $\check{\gamma}_{s,t}$ and $\check{\gamma}_{t,s}$ are because of (3.26) with these parameters and

$$\check{a} = \check{a}_{s,t} = k_0 \sin(\frac{\theta}{2}) = \sqrt{k_0^2 - a^2}$$

of the form of $\check{\gamma}_1$ and $\check{\gamma}_2$.

Since the curves $\gamma_{s,t}$ and $\gamma_{t,s}$ as well as $\check{\gamma}_{s,t}$ and $\check{\gamma}_{t,s}$ fulfill by construction the equations (3.17) and (3.29), and $(\gamma_\ell)_{\ell=1}^2$ and $(\check{\gamma}_\ell)_{\ell=1}^2$ are by assumption the only elliptic arcs of this form with the properties (3.34) and (3.35), we have that $\gamma_1 = \gamma_{s,t}$, $\gamma_2 = \gamma_{t,s}$, $\check{\gamma}_1 = \check{\gamma}_{s,t}$, and $\check{\gamma}_2 = \check{\gamma}_{t,s}$.

We note that the two pairs of curves can in general not be interchanged because in (3.34) the curve γ_1 is traversed counter-clockwise and γ_2 is traversed with $\beta \mapsto \gamma_2(-\beta)$ clockwise, whereas in (3.35) both $\check{\gamma}_1$ and $\check{\gamma}_2$ are traversed counter-clockwise.

Thus, we can uniquely determine the three Euler angles φ , θ , and ψ from (3.38) and (3.39), and we find (3.36). \square

Remark 3.10 Because the curves $\check{\gamma}_\ell$ in (3.35) are traversed in the same direction and the curves γ_ℓ in (3.34) in the opposite direction, they can be distinguished. Hence, in Theorem 3.9 it suffices if only one of the equations (3.34) and (3.35) is uniquely fulfilled in order to obtain the reconstruction of $R_s^\top R_t$. This then also implies that the other of these two equations holds. \square

Thus, we can read off the relative rotation $R_s^\top R_t$, which the object undergoes from time t to time s , from two data sets ν_s and ν_t only. This is in contrast to the common line method for the ray transform [7], which requires to detect the intersection of pairwise common lines in images of at least three different times in order to calculate the relative rotations, see Figure 1. This is also apparent from the fact that our common circle formulation contains the three Euler angles from the three dimensional manifold $\text{SO}(3)$ as parameters, whereas in the common line method for the ray transform there are only the two parameters parametrizing the lines through the origin.

Nevertheless, the reconstructability relies on the uniqueness of the elliptic arcs γ_1 and γ_2 with the property (3.34), which can easily fail if the function f has too much symmetry. If f is, for example, rotationally invariant, then so is its Fourier transform $\mathcal{F}[f]$ and therefore $\nu_s = \nu_t$ for all $s, t \in [0, T]$, which clearly makes it impossible to reconstruct any rotation. In the generic case, however, we expect that this problem does not occur and neither does it in our numerical examples.

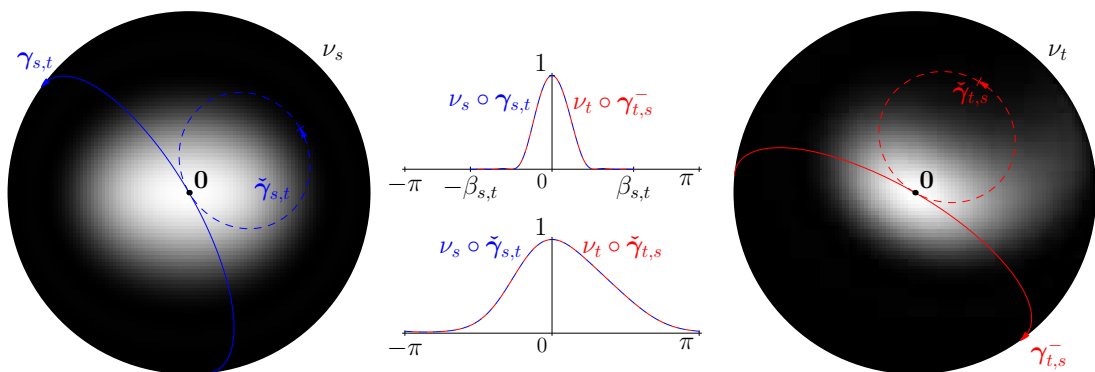


Figure 5: Scaled squared energies ν_s and ν_t for a characteristic function $f := \chi_E$ of an ellipsoid $E \subset \mathbb{R}^3$ with the relative rotation $R_s^\top R_t = R^{(3)}(\frac{\pi}{6})R^{(2)}(\frac{\pi}{4})R^{(3)}(\frac{2\pi}{3})$ with the paths of the corresponding two elliptic arcs $\gamma_{s,t}$ and $\gamma_{t,s}^-$, where $\gamma_{t,s}^-$ denotes the reversed elliptic arc $\gamma_{t,s}^-(\beta) := \gamma_{t,s}(-\beta)$, and their dual arcs $\check{\gamma}_{s,t}$ and $\check{\gamma}_{t,s}$. The relations (3.17) and (3.29) are verified in the center by plotting the values of ν_s and ν_t along the arcs.

3.2 Parametrization via Stereographic Projection

To avoid the necessity to detect elliptic arcs in the images, we may use a different parametrization of the hemispheres in which the arcs become straight lines. Such a parametrization is provided by the stereographic projection $\pi_t: \partial\mathcal{B}_{k_0}^3(-k_0 R_t e^3) \setminus \{0\} \rightarrow \mathcal{P}_t$ of the hemisphere $\mathcal{H}_t \setminus \{0\}$ of the sphere $\partial\mathcal{B}_{k_0}^3(-k_0 R_t e^3)$ from the origin onto the equatorial plane

$$\mathcal{P}_t := \{\mathbf{x} \in \mathbb{R}^3 : \langle \mathbf{x}, R_t e^3 \rangle = -k_0\}.$$

This maps every circle $\partial\mathcal{B}_{k_0}^3(-k_0 R_s e^3) \cap \partial\mathcal{B}_{k_0}^3(-k_0 R_t e^3)$ (as it passes through the origin, which could be defined to be mapped to infinity) to a straight line in \mathcal{P}_t .

The stereographic projection π_t of a point $\mathbf{x} \in \partial\mathcal{B}_{k_0}^3(-k_0 R_t e^3) \setminus \{0\}$ is hereby defined as the intersection of the line through $\mathbf{0}$ and \mathbf{x} with the plane \mathcal{P}_t . In particular, we have for $t = 0$ where the rotation is $R_0 = I$ that

$$\begin{aligned} \pi_0: \partial\mathcal{B}_{k_0}^3(-k_0 e^3) \setminus \{0\} &\rightarrow \mathcal{P}_0, \\ \mathbf{x} \mapsto \pi_0(\mathbf{x}) &:= \left(-k_0 \frac{x_1}{x_3}, -k_0 \frac{x_2}{x_3}, -k_0 \right)^\top = -k_0 \frac{\mathbf{x}}{x_3}. \end{aligned} \quad (3.40)$$

The stereographic projection π_t for general $t \in [0, T]$ is then obtained by rotating a point $\mathbf{x} \in \partial\mathcal{B}_{k_0}^3(-k_0 R_t e^3)$ first to $\partial\mathcal{B}_{k_0}^3(-k_0 e^3)$ and rotating the projected point in \mathcal{P}_0 back to \mathcal{P}_t , i.e.,

$$\pi_t(\mathbf{x}) := R_t \pi_0(R_t^\top \mathbf{x}).$$

The following lemma shows that we can write all the projections π_t as restrictions of the function

$$\begin{aligned} \pi: \mathbb{R}^3 \setminus \{\mathbf{0}\} &\rightarrow \mathbb{R}^3 \setminus \{\mathbf{0}\}, \\ \mathbf{x} &\mapsto \pi(\mathbf{x}) := 2k_0^2 \frac{\mathbf{x}}{\|\mathbf{x}\|^2}, \end{aligned} \quad (3.41)$$

whose inverse is given by $\pi^{-1} = \pi$.

Lemma 3.11 *For every $t \in [0, T]$, we have*

$$\pi_t(\mathbf{x}) = \pi(\mathbf{x}) \quad \text{for all } \mathbf{x} \in \partial\mathcal{B}_{k_0}^3(-k_0 R_t \mathbf{e}^3) \setminus \{\mathbf{0}\}.$$

Proof: Let $\mathbf{x} \in \partial\mathcal{B}_{k_0}^3(-k_0 R_t \mathbf{e}^3) \setminus \{\mathbf{0}\}$. Then we obtain

$$0 = \left\| \mathbf{x} + k_0 R_t \mathbf{e}^3 \right\|^2 - k_0^2 = \|\mathbf{x}\|^2 + 2k_0 \langle R_t^\top \mathbf{x}, \mathbf{e}^3 \rangle$$

and therefore

$$\pi_t(\mathbf{x}) = R_t \pi_0(R_t^\top \mathbf{x}) = -k_0 R_t \frac{R_t^\top \mathbf{x}}{\langle R_t^\top \mathbf{x}, \mathbf{e}^3 \rangle} = 2k_0^2 \frac{\mathbf{x}}{\|\mathbf{x}\|^2} = \pi(\mathbf{x}). \quad \square$$

We now consider for arbitrary $t \in [0, T]$ the function

$$\begin{aligned} \tau: \mathcal{B}_{k_0}^2 \setminus \{\mathbf{0}\} &\rightarrow \mathbb{R}^2 \setminus \overline{\mathcal{B}_{k_0}^2}, \\ \mathbf{k} &\mapsto \tau(\mathbf{k}) := P(R_t^\top \pi_t(R_t \mathbf{h}(\mathbf{k}))) = P(\pi_0(\mathbf{h}(\mathbf{k}))) = \frac{k_0}{k_0 - \kappa(\mathbf{k})} \mathbf{k}, \end{aligned} \quad (3.42)$$

which describes the change from the parametrization via $R_t \mathbf{h}$ to the one via stereographic projection and is conveniently independent of the choice of $t \in [0, T]$. It maps by definition the data point \mathbf{k} by the parametrization $R_t \mathbf{h}$ onto the hemisphere \mathcal{H}_t , stereographically projects it to \mathcal{P}_t (with image $\mathcal{P}_t \setminus \overline{\mathcal{B}_{k_0}^3(-k_0 R_t \mathbf{e}^3)}$), and extracts the two components in the plane by rotating it to \mathcal{P}_0 and orthogonally projecting it with P to the first two components, see (3.10). Therefore it maps every elliptic arc $\gamma_{t,s}$ to a straight line. The codomain of τ is chosen so that τ is bijective, and its inverse is given by

$$\tau^{-1}(\mathbf{y}) = \frac{2k_0^2}{k_0^2 + \|\mathbf{y}\|^2} \mathbf{y}, \quad \mathbf{y} \in \mathbb{R}^2 \setminus \overline{\mathcal{B}_{k_0}^2}.$$

Lemma 3.12 *Let $s, t \in [0, T]$ be such that $R_s \mathbf{e}^3 \neq \pm R_t \mathbf{e}^3$ and $(\varphi, \theta, \psi) \in (\mathbb{R}/(2\pi\mathbb{Z})) \times [0, \pi] \times (\mathbb{R}/(2\pi\mathbb{Z}))$ be the Euler angles of the rotation $R_s^\top R_t$ as in (3.18).*

(i) *The elliptic arc $\gamma_{s,t}$ defined in (3.12) fulfills*

$$\tau(\gamma_{s,t}(\beta)) = -k_0 \tan\left(\frac{\theta}{2}\right) \begin{pmatrix} \cos(\varphi) \\ \sin(\varphi) \end{pmatrix} + \frac{k_0}{\cos(\frac{\theta}{2})} \cot\left(\frac{\beta}{2}\right) \begin{pmatrix} -\sin(\varphi) \\ \cos(\varphi) \end{pmatrix}, \quad \beta \in J_{s,t} \setminus \{0\}. \quad (3.43)$$

(ii) *The dual elliptic arc $\check{\gamma}_{s,t}$ given by (3.25) fulfills*

$$\tau(\check{\gamma}_{s,t}(\beta)) = k_0 \cot\left(\frac{\theta}{2}\right) \begin{pmatrix} \cos(\varphi) \\ \sin(\varphi) \end{pmatrix} - \frac{k_0}{\sin(\frac{\theta}{2})} \cot\left(\frac{\beta}{2}\right) \begin{pmatrix} -\sin(\varphi) \\ \cos(\varphi) \end{pmatrix}, \quad \beta \in \check{J}_{s,t} \setminus \{0\}. \quad (3.44)$$

Proof:

(i) We use (3.11) to write

$$\tau(\gamma_{s,t}(\beta)) = P(\boldsymbol{\pi}_0(\mathbf{h}(\gamma_{s,t}(\beta)))) = P(\boldsymbol{\pi}_0(R_s^\top \boldsymbol{\sigma}_{s,t}(\beta))).$$

Plugging in the expression (3.5) for the circular arc $\boldsymbol{\sigma}_{s,t}$ and the definition (3.40) of the function $\boldsymbol{\pi}_0$, we arrive at

$$\tau(\gamma_{s,t}(\beta)) = k_0 \frac{a_{s,t}(\cos(\beta) - 1)P(R_s^\top \mathbf{v}_{s,t}^1) + a_{s,t} \sin(\beta)P(R_s^\top \mathbf{v}_{s,t}^2)}{\frac{k_0}{2}(1 - \cos(\beta))(1 + \langle R_s \mathbf{e}^3, R_t \mathbf{e}^3 \rangle)}.$$

As in Lemma 3.2, where we already calculated the projections of the basis vectors $\mathbf{v}_{s,t}^1$ and $\mathbf{v}_{s,t}^2$ in (3.15), we can rewrite this in the form

$$\tau(\gamma_{s,t}(\beta)) = 2 \frac{\tilde{a}_{s,t}(\cos(\beta) - 1)\mathbf{w}_{s,t}^1 + a_{s,t} \sin(\beta)\mathbf{w}_{s,t}^2}{(1 - \cos(\beta))(1 + \langle R_s \mathbf{e}^3, R_t \mathbf{e}^3 \rangle)}.$$

Using $1 + \langle R_s \mathbf{e}^3, R_t \mathbf{e}^3 \rangle = \frac{1}{2} \|R_s \mathbf{e}^3 + R_t \mathbf{e}^3\|^2 = \frac{2}{k_0^2} a_{s,t}^2$ and the trigonometric identity $\frac{\sin(\beta)}{1 - \cos(\beta)} = \cot(\frac{\beta}{2})$, this becomes

$$\tau(\gamma_{s,t}(\beta)) = -\frac{k_0^2 \tilde{a}_{s,t}}{a_{s,t}^2} \mathbf{w}_{s,t}^1 + \frac{k_0^2}{a_{s,t}} \cot(\frac{\beta}{2}) \mathbf{w}_{s,t}^2.$$

Inserting the expressions for the parameters in Euler angles as in Lemma 3.4, we obtain (3.43).

(ii) In the same way, we find with the results and the notation of Lemma 3.5

$$\tau(\check{\gamma}_{s,t}(\beta)) = P(\boldsymbol{\pi}_0(R_s^\top \check{\boldsymbol{\sigma}}_{s,t}(\beta))) = -k_0 \frac{\check{a}_{s,t}(\cos(\beta) - 1)P(R_s^\top \mathbf{v}_{s,t}^3) - \check{a}_{s,t} \sin(\beta)P(R_s^\top \mathbf{v}_{s,t}^2)}{\frac{k_0}{2}(\cos(\beta) - 1)(1 - \langle R_s \mathbf{e}^3, R_t \mathbf{e}^3 \rangle)}.$$

Using (3.15) and (3.27) to express the projections of the basis vectors $\mathbf{v}_{s,t}^2$ and $\mathbf{v}_{s,t}^3$, we get with $1 - \langle R_s \mathbf{e}^3, R_t \mathbf{e}^3 \rangle = \frac{1}{2} \|R_s \mathbf{e}^3 - R_t \mathbf{e}^3\|^2 = \frac{2}{k_0^2} \check{a}_{s,t}^2$ that

$$\tau(\check{\gamma}_{s,t}(\beta)) = k_0^2 \frac{\check{a}_{s,t}}{\check{a}_{s,t}^2} \mathbf{w}_{s,t}^1 - \frac{k_0^2}{\check{a}_{s,t}} \cot(\frac{\beta}{2}) \mathbf{w}_{s,t}^2.$$

Inserting the expressions for the parameters in Euler angles as in Lemma 3.4 and Lemma 3.5, this becomes (3.44). \square

From the definitions of the intervals $J_{s,t}$ and $\check{J}_{s,t}$, the functions $\tau \circ \gamma_{s,t}: J_{s,t} \setminus \{0\} \rightarrow \mathbb{R}^2 \setminus \overline{\mathcal{B}_{k_0}^2}$ from (3.43) and $\tau \circ \check{\gamma}_{s,t}: \check{J}_{s,t} \setminus \{0\} \rightarrow \mathbb{R}^2 \setminus \overline{\mathcal{B}_{k_0}^2}$ from (3.44) can be seen to parametrize the parts of straight lines in \mathbb{R}^2 which are outside the ball $\overline{\mathcal{B}_{k_0}^2}$, see Figure 6.

Thus, looking for straight lines in the transformed scaled squared energy $\hat{\nu}_t: \mathbb{R}^2 \setminus \overline{\mathcal{B}_{k_0}^2} \rightarrow [0, \infty)$, defined by

$$\hat{\nu}_t := \nu_t \circ \tau^{-1} \quad \text{for all } t \in [0, T], \quad (3.45)$$

we can recover the Euler angles as before. This is summarized in the following corollary.

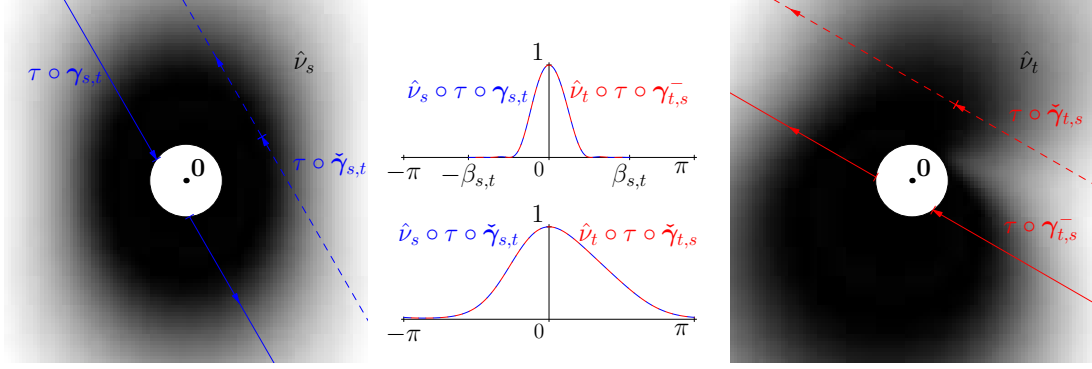


Figure 6: Transformed scaled squared energies \hat{v}_s and \hat{v}_t , see (3.45), for the same situation as in Figure 5 and the paths of the corresponding two straight lines $\tau \circ \gamma_{s,t}$ and $\tau \circ \gamma_{t,s}^-$ (the minus again indicating the reversed direction) and their dual straight lines $\tau \circ \check{\gamma}_{s,t}$ and $\tau \circ \check{\gamma}_{t,s}$. The values of \hat{v}_s and \hat{v}_t along the lines are plotted in the center of the figure.

Corollary 3.13 *Let $s, t \in [0, T]$ be such that $R_s e^3 \neq \pm R_t e^3$ and assume that there uniquely exist two pairs $(\Gamma_\ell)_{\ell=1}^2$ and $(\check{\Gamma}_\ell)_{\ell=1}^2$ of straight lines of the form*

$$\Gamma_\ell: \mathbb{R} \rightarrow \mathbb{R}^2, \quad \Gamma_\ell(\xi) := -b\mathbf{w}_\ell^1 + \xi\mathbf{w}_\ell^2, \quad \text{and} \quad (3.46)$$

$$\check{\Gamma}_\ell: \mathbb{R} \rightarrow \mathbb{R}^2, \quad \check{\Gamma}_\ell(\xi) := \frac{k_0^2}{b}\mathbf{w}_\ell^1 - \xi\mathbf{w}_\ell^2, \quad \ell \in \{1, 2\}, \quad (3.47)$$

for some parameter $b \in (0, \infty)$ and two positively oriented, orthonormal bases $(\mathbf{w}_1^j)_{j=1}^2$ and $(\mathbf{w}_2^j)_{j=1}^2$ of \mathbb{R}^2 such that we have for the transformed scaled squared energy \hat{v} that

$$\begin{aligned} \hat{v}_s(\Gamma_1(\xi)) &= \hat{v}_t(\Gamma_2(-\xi)) \quad \text{for all } \xi \in \mathbb{R} \quad \text{with } \xi^2 > k_0^2 - b^2, \\ \hat{v}_s(\check{\Gamma}_1(\xi)) &= \hat{v}_t(\check{\Gamma}_2(\xi)) \quad \text{for all } \xi \in \mathbb{R} \quad \text{with } \xi^2 > k_0^2 - k_0^4 b^{-2}. \end{aligned}$$

Then the relative rotation is given by

$$R_s^\top R_t = R^{(3)}(\arg(\mathbf{w}_1^1))R^{(2)}(2 \arctan(\frac{b}{k_0}))R^{(3)}(\pi - \arg(\mathbf{w}_2^1)). \quad (3.48)$$

Proof: We parametrize the matrix $R_s^\top R_t$ in Euler angles $(\varphi, \theta, \psi) \in (\mathbb{R}/(2\pi\mathbb{Z})) \times [0, \pi] \times (\mathbb{R}/(2\pi\mathbb{Z}))$ as in (3.18) and get for the representation of $R_t^\top R_s$ in Euler angles the formula (3.37). Then, we consider the straight lines $\tau \circ \gamma_{s,t}$ and $\tau \circ \check{\gamma}_{s,t}$, given by (3.43) and (3.44), where $\gamma_{s,t}$ and $\check{\gamma}_{s,t}$ denote the elliptic arcs introduced in (3.12) and (3.25), and reparametrize them via the functions

$$\begin{aligned} \Xi: J_{s,t} \setminus \{0\} &\rightarrow \{\xi \in \mathbb{R} : \xi^2 > k_0^2 - k_0^2 \tan^2(\frac{\theta}{2})\}, \quad \Xi(\beta) := \frac{k_0}{\cos(\frac{\beta}{2})} \cot(\frac{\beta}{2}), \quad \text{and} \\ \check{\Xi}: \check{J}_{s,t} \setminus \{0\} &\rightarrow \{\xi \in \mathbb{R} : \xi^2 > k_0^2 - k_0^2 \cot^2(\frac{\theta}{2})\}, \quad \check{\Xi}(\beta) := \frac{k_0}{\sin(\frac{\beta}{2})} \cot(\frac{\beta}{2}), \end{aligned}$$

which are seen to be bijective by using that $\beta \in J_{s,t}$ is by definition (3.7) for $\beta \in (-\pi, \pi]$ equivalent to $\cos(\beta) > \frac{\cos(\theta)-1}{\cos(\theta)+1}$, which is equivalent to $\cot^2(\frac{\beta}{2}) = \frac{1+\cos(\beta)}{1-\cos(\beta)} > \cos(\theta)$, and therefore to

$$(\Xi(\beta))^2 + k_0^2 \tan^2(\frac{\theta}{2}) > \frac{k_0^2}{\cos^2(\frac{\theta}{2})}(\cos^2(\frac{\theta}{2}) - \sin^2(\frac{\theta}{2})) + k_0^2 \tan^2(\frac{\theta}{2}) = k_0^2.$$

Analogously, we find that $\beta \in \check{J}_{s,t}$ is by definition (3.23) for $\beta \in (-\pi, \pi]$ equivalent to $\cos(\beta) > \frac{\cos(\theta)+1}{\cos(\theta)-1}$, which is equivalent to $\cot^2(\frac{\beta}{2}) = \frac{1+\cos(\beta)}{1-\cos(\beta)} > -\cos(\theta)$, and therefore to

$$(\check{\Xi}(\beta))^2 + k_0^2 \cot^2(\frac{\theta}{2}) > \frac{k_0^2}{\sin^2(\frac{\theta}{2})}(\sin^2(\frac{\theta}{2}) - \cos^2(\frac{\theta}{2})) + k_0^2 \cot^2(\frac{\theta}{2}) = k_0^2.$$

Then, according to (3.43), the curves $\tau \circ \gamma_{s,t} \circ \Xi^{-1}$ and $\tau \circ \gamma_{t,s} \circ \Xi^{-1}$ are with

$$b = k_0 \tan\left(\frac{\theta}{2}\right), \quad \mathbf{w}_1^1 = \mathbf{w}_{s,t}^1 = \begin{pmatrix} \cos(\varphi) \\ \sin(\varphi) \end{pmatrix}, \quad \text{and} \quad \mathbf{w}_2^1 = \mathbf{w}_{t,s}^1 = \begin{pmatrix} \cos(\pi - \psi) \\ \sin(\pi - \psi) \end{pmatrix} \quad (3.49)$$

on the set $X := \{\xi \in \mathbb{R} : \xi^2 > k_0^2 - b^2\}$ of the form (3.46); and according to (3.44), the dual curves $\tau \circ \check{\gamma}_{s,t} \circ \check{\Xi}^{-1}$ and $\tau \circ \check{\gamma}_{t,s} \circ \check{\Xi}^{-1}$ are with this on the set $\check{X} := \{\xi \in \mathbb{R} : \xi^2 > k_0^2 - k_0^4 b^{-2}\}$ of the form (3.47). Moreover, these curves fulfill according to (3.17) and (3.29)

$$\begin{aligned} \hat{\nu}_s(\tau(\gamma_{s,t}(\Xi^{-1}(\xi)))) &= \nu_s(\gamma_{s,t}(\Xi^{-1}(\xi))) = \nu_t(\gamma_{t,s}(-\Xi^{-1}(\xi))) = \hat{\nu}_t(\tau(\gamma_{t,s}(\Xi^{-1}(-\xi))))), & \xi \in X, \\ \hat{\nu}_s(\tau(\check{\gamma}_{s,t}(\check{\Xi}^{-1}(\xi)))) &= \nu_s(\check{\gamma}_{s,t}(\check{\Xi}^{-1}(\xi))) = \nu_t(\check{\gamma}_{t,s}(\check{\Xi}^{-1}(\xi))) = \hat{\nu}_t(\tau(\check{\gamma}_{t,s}(\check{\Xi}^{-1}(\xi))))), & \xi \in \check{X}. \end{aligned}$$

The uniqueness of the pairs $(\Gamma_\ell)_{\ell=1}^2$ and $(\check{\Gamma}_\ell)_{\ell=1}^2$ therefore implies $\Gamma_1 = \tau \circ \gamma_{s,t} \circ \Xi^{-1}$, $\Gamma_2 = \tau \circ \gamma_{t,s} \circ \Xi^{-1}$, $\check{\Gamma}_1 = \tau \circ \check{\gamma}_{s,t} \circ \check{\Xi}^{-1}$, and $\check{\Gamma}_2 = \tau \circ \check{\gamma}_{t,s} \circ \check{\Xi}^{-1}$, so that we can read off the Euler angles from the correspondencies (3.49), giving us the reconstruction (3.48). \square

4 Infinitesimal Common Circle Method

In this section, we make the additional assumption that the rotations R_t to which the object is exposed via the transformation (2.11) depend smoothly on the time $t \in [0, T]$, i.e., we assume that $R \in C^1([0, T] \rightarrow \text{SO}(3))$. Since the fact that the scattering potential f has compact support implies by the Paley–Wiener theorem that $\mathcal{F}[f] \in C^\infty(\mathbb{R}^3 \rightarrow \mathbb{C})$, we thus have that ν is continuously differentiable both in time and space.

In this setting we can describe the relative rotation $R_s^\top R_t$ between two time steps $s, t \in [0, T]$ in the limit $s \rightarrow t$ by the derivative $(R_t')^\top R_t = (R_t^\top R_t')^\top$, where R_t' denotes the time derivative of R at $t \in [0, T]$. Since taking the derivative of the defining identity $R_t^\top R_t = I$ of orthogonal matrices with respect to t gives us the relation $R_t^\top R_t' + (R_t^\top R_t')^\top = 0$, the *angular velocity matrix* $W_t := R_t^\top R_t'$ is skew-symmetric. Thus, we can describe W_t with only three parameters. The *angular velocity* $\boldsymbol{\omega} : [0, T] \rightarrow \mathbb{R}^3$ of the rotational motion R , cf. [23, Chapter VI], is defined by

$$R_t^\top R_t' \mathbf{y} = \boldsymbol{\omega}_t \times \mathbf{y}, \quad \text{that is,} \quad W_t = \begin{pmatrix} 0 & -\omega_{t,3} & \omega_{t,2} \\ \omega_{t,3} & 0 & -\omega_{t,1} \\ -\omega_{t,2} & \omega_{t,1} & 0 \end{pmatrix} \quad \text{for all } t \in [0, T], \quad \mathbf{y} \in \mathbb{R}^3, \quad (4.1)$$

where we write $\boldsymbol{\omega}_t = (\omega_{t,1}, \omega_{t,2}, \omega_{t,3})^\top$.

In the following, we want to reconstruct the angular velocity $\boldsymbol{\omega}_t$ of the rigid motion at a time $t \in [0, T]$ from the behavior of the data ν in the vicinity of the time t , more precisely from the first derivatives of ν at the time t utilizing a similar approach as it was applied for the ray transform in [7].

For the reconstruction, it is convenient to express $\boldsymbol{\omega}_t$ in cylindrical coordinates

$$\boldsymbol{\omega}_t = \begin{pmatrix} \rho_t \phi_t \\ \zeta_t \end{pmatrix} \quad (4.2)$$

with the azimuth direction $\phi_t \in \mathbb{S}_+^1 := \{(\cos(\alpha), \sin(\alpha))^\top : \alpha \in [0, \pi)\}$, the cylindrical radius $\rho_t \in \mathbb{R}$, and the third component $\zeta_t \in \mathbb{R}$. Note that, in contrast to conventional cylindrical coordinates, we allow negative radii ρ_t , but restrict in exchange ϕ_t to \mathbb{S}_+^1 .

To obtain the reconstruction formula, we consider for values $s, t \in [0, T]$ with $R_s e^3 \neq \pm R_t e^3$ again the elliptic arcs $\gamma_{s,t}$ in (3.12) fulfilling the identity

$$\nu_s(\gamma_{s,t}(\beta)) = \nu_t(\gamma_{t,s}(-\beta)), \quad (4.3)$$

in (3.17). Taking therein for fixed $t \in [0, T]$ the limit $s \rightarrow t$, we find that the relation

$$\lim_{s \rightarrow t} \frac{\nu_s(\gamma_{s,t}(\beta)) - \nu_t(\gamma_{t,s}(-\beta))}{s - t} = 0 \quad (4.4)$$

holds, which gives us a relation between the first order derivatives of the function $(t, \mathbf{k}) \mapsto \nu_t(\mathbf{k})$ involving only the angular velocity $\boldsymbol{\omega}_t$ of the rotations at the time t . As we will see, this first order part of (4.3) contains enough information to recover this angular velocity and therefore the whole rotations. This method can thus be seen as an infinitesimal version of Theorem 3.9.

Instead of rewriting the relation (4.4) directly by expanding the functions in Taylor series in the variable s around the point t , we will simply verify the resulting relation.

Lemma 4.1 *Let the rotations $R \in C^1([0, T] \rightarrow \text{SO}(3))$ be continuously differentiable and the associated angular velocities $\boldsymbol{\omega}: [0, T] \rightarrow \mathbb{R}^3$ be written in cylindrical coordinates (4.2). Then we have for every $r \in (-k_0, k_0)$ the relation*

$$\partial_t \nu_t(r\boldsymbol{\phi}_t) = \left(\rho_t \left(k_0 - \sqrt{k_0^2 - r^2} \right) + r\zeta_t \right) \left\langle \nabla \nu_t(r\boldsymbol{\phi}_t), \begin{pmatrix} -\phi_{t,2} \\ \phi_{t,1} \end{pmatrix} \right\rangle \quad (4.5)$$

for the scaled squared energy ν , where $\partial_t \nu_t$ denotes the partial derivative of ν_t with respect to t .

Proof: We consider the continuously differentiable function $H: [0, T] \times \mathcal{B}_{k_0}^2 \rightarrow \mathbb{R}^3$ defined by $H(t, \mathbf{k}) := R_t \mathbf{h}(\mathbf{k})$ with \mathbf{h} being the parametrization from (2.7). Then we get with the definition (4.1) of the angular velocity $\boldsymbol{\omega}$ for the partial derivative of H with respect to the first argument at the point $r\boldsymbol{\phi}_t$ the relation

$$\partial_t H(t, r\boldsymbol{\phi}_t) = R_t(\boldsymbol{\omega}_t \times \mathbf{h}(r\boldsymbol{\phi}_t)) = R_t \begin{pmatrix} \omega_{t,2} h_3(r\boldsymbol{\phi}_t) - r\omega_{t,3} \phi_{t,2} \\ -\omega_{t,1} h_3(r\boldsymbol{\phi}_t) + r\omega_{t,3} \phi_{t,1} \\ r(\omega_{t,1} \phi_{t,2} - \omega_{t,2} \phi_{t,1}) \end{pmatrix}.$$

Inserting the expression (4.2) of $\boldsymbol{\omega}$ in cylindrical coordinates and using that, according to (2.7), $h_3(r\boldsymbol{\phi}_t) = \sqrt{k_0^2 - r^2} - k_0^2$, this becomes

$$\partial_t H(t, r\boldsymbol{\phi}_t) = \left(\rho_t \left(k_0 - \sqrt{k_0^2 - r^2} \right) + r\zeta_t \right) R_t \begin{pmatrix} -\phi_{t,2} \\ \phi_{t,1} \\ 0 \end{pmatrix}.$$

For the derivative of H with respect to \mathbf{k} , denoting by DH the corresponding Jacobi matrix of H , we find

$$DH(t, r\boldsymbol{\phi}_t) \begin{pmatrix} -\phi_{t,2} \\ \phi_{t,1} \end{pmatrix} = R_t \begin{pmatrix} 1 & 0 \\ 0 & 1 \\ \frac{-r\phi_{t,1}}{\sqrt{k_0^2 - r^2}} & \frac{-r\phi_{t,2}}{\sqrt{k_0^2 - r^2}} \end{pmatrix} \begin{pmatrix} -\phi_{t,2} \\ \phi_{t,1} \end{pmatrix} = R_t \begin{pmatrix} -\phi_{t,2} \\ \phi_{t,1} \\ 0 \end{pmatrix}.$$

Therefore, we have that

$$\partial_t H(t, r\boldsymbol{\phi}_t) = \left(\rho_t \left(k_0 - \sqrt{k_0^2 - r^2} \right) + r\zeta_t \right) DH(t, r\boldsymbol{\phi}_t) \begin{pmatrix} -\phi_{t,2} \\ \phi_{t,1} \end{pmatrix},$$

which implies by $\nu_t(\mathbf{k}) = |\mathcal{F}[f](H(t, \mathbf{k}))|^2$ the equation (4.5) for ν . \square

In the parametrization via the stereographic projection discussed in [Section 3.2](#), the coefficient of the spatial derivative in [\(4.5\)](#) becomes affine.

Lemma 4.2 *Let the rotations $R \in C^1([0, T] \rightarrow \text{SO}(3))$ be continuously differentiable and the associated angular velocities $\boldsymbol{\omega}: [0, T] \rightarrow \mathbb{R}^3$ be written in cylindrical coordinates [\(4.2\)](#). Then, the transformed scaled squared energy $\hat{\nu}$, defined in [\(3.45\)](#), satisfies for every $\hat{r} \in \mathbb{R} \setminus [-k_0, k_0]$ the relation*

$$\partial_t \hat{\nu}_t(\hat{r}\boldsymbol{\phi}_t) = (k_0\rho_t + \hat{r}\zeta_t) \left\langle \nabla \hat{\nu}_t(\hat{r}\boldsymbol{\phi}_t), \begin{pmatrix} -\phi_{t,2} \\ \phi_{t,1} \end{pmatrix} \right\rangle. \quad (4.6)$$

Proof: The transformed data $\hat{\nu}$ is given by

$$\hat{\nu}_t(\mathbf{y}) = \nu_t(\tau^{-1}(\mathbf{y})) = \left| \mathcal{F}[f](R_t \mathbf{h}(\tau^{-1}(\mathbf{y}))) \right|^2.$$

Using now that we have by definition [\(3.40\)](#) of $\boldsymbol{\pi}_0$ and definition [\(3.42\)](#) of τ that

$$\begin{pmatrix} \tau(\tau^{-1}(\mathbf{y})) \\ -k_0 \end{pmatrix} = \boldsymbol{\pi}_0(\mathbf{h}(\tau^{-1}(\mathbf{y}))) = R_t^\top \boldsymbol{\pi}_t(R_t \mathbf{h}(\tau^{-1}(\mathbf{y}))),$$

we have with [Lemma 3.11](#) and $\boldsymbol{\pi}^{-1} = \boldsymbol{\pi}$ the relation

$$\hat{\nu}_t(\mathbf{y}) = \left| \mathcal{F}[f](R_t \mathbf{h}(\tau^{-1}(\mathbf{y}))) \right|^2 = \left| \mathcal{F}[f](\boldsymbol{\pi}(\hat{H}(t, \mathbf{y}))) \right|^2 \quad (4.7)$$

with the function $\hat{H}: [0, T] \times \mathbb{R}^2 \setminus \overline{\mathcal{B}_{k_0}^2} \rightarrow \mathbb{R}^3$, $\hat{H}(t, \mathbf{y}) := R_t \begin{pmatrix} \mathbf{y} \\ -k_0 \end{pmatrix}$.

Since the partial derivative $\partial_t \hat{H}$ of \hat{H} with respect to t fulfills

$$\partial_t \hat{H}(t, \hat{r}\boldsymbol{\phi}_t) = R_t \left(\boldsymbol{\omega}_t \times \begin{pmatrix} \hat{r}\boldsymbol{\phi}_t \\ -k_0 \end{pmatrix} \right) = R_t \left(\begin{pmatrix} \rho_t \boldsymbol{\phi}_t \\ \zeta_t \end{pmatrix} \times \begin{pmatrix} \hat{r}\boldsymbol{\phi}_t \\ -k_0 \end{pmatrix} \right) = (k_0\rho_t + \hat{r}\zeta_t) R_t \begin{pmatrix} -\phi_{t,2} \\ \phi_{t,1} \\ 0 \end{pmatrix}$$

and the Jacobi matrix $D\hat{H}$ of \hat{H} with respect to \mathbf{y} satisfies

$$D\hat{H}(t, \hat{r}\boldsymbol{\phi}_t) \begin{pmatrix} -\phi_{t,2} \\ \phi_{t,1} \end{pmatrix} = R_t \begin{pmatrix} 1 & 0 \\ 0 & 1 \end{pmatrix} \begin{pmatrix} -\phi_{t,2} \\ \phi_{t,1} \end{pmatrix} = R_t \begin{pmatrix} -\phi_{t,2} \\ \phi_{t,1} \\ 0 \end{pmatrix},$$

we have

$$\partial_t \hat{H}(t, \hat{r}\boldsymbol{\phi}_t) = (k_0\rho_t + \hat{r}\zeta_t) D\hat{H}(t, \hat{r}\boldsymbol{\phi}_t) \begin{pmatrix} -\phi_{t,2} \\ \phi_{t,1} \end{pmatrix},$$

which implies with [\(4.7\)](#) directly [\(4.6\)](#). \square

This gives rise to the following reconstruction method, which we can formulate either in terms of the scaled squared energy ν or, by switching to the stereographic parametrization, in terms of the transformed scaled squared energy $\hat{\nu}$. To obtain a unique reconstruction, we require that the data is such that the equations [\(4.5\)](#) and [\(4.6\)](#) are only fulfilled if ρ_t , $\boldsymbol{\phi}_t$, and ζ_t are the values from the angular velocity.

Theorem 4.3 *Let the rotations $R \in C^1([0, T] \rightarrow \text{SO}(3))$ be continuously differentiable and the associated angular velocities $\boldsymbol{\omega}: [0, T] \rightarrow \mathbb{R}^3$ be written in cylindrical coordinates [\(4.2\)](#). Let further $t \in [0, T]$ be such that there is a unique direction $\tilde{\boldsymbol{\phi}}_t \in \mathbb{S}_+^1$ with the property that there exist parameters $\tilde{\rho}_t, \tilde{\zeta}_t \in \mathbb{R}$ with*

$$\partial_t \nu_t(r\tilde{\boldsymbol{\phi}}_t) = \left(\tilde{\rho}_t \left(k_0 - \sqrt{k_0^2 - r^2} \right) + r\tilde{\zeta}_t \right) \left\langle \nabla \nu_t(r\tilde{\boldsymbol{\phi}}_t), \begin{pmatrix} -\tilde{\phi}_{t,2} \\ \tilde{\phi}_{t,1} \end{pmatrix} \right\rangle \quad \text{for all } r \in (-k_0, k_0), \quad (4.8)$$

for the scaled squared energy ν_t or equivalently,

$$\partial_t \hat{\nu}_t(\hat{r}\tilde{\boldsymbol{\phi}}_t) = (k_0\tilde{\rho}_t + \hat{r}\tilde{\zeta}_t) \left\langle \nabla \hat{\nu}_t(\hat{r}\tilde{\boldsymbol{\phi}}_t), \begin{pmatrix} -\tilde{\phi}_{t,2} \\ \tilde{\phi}_{t,1} \end{pmatrix} \right\rangle \quad \text{for all } \hat{r} \in \mathbb{R} \setminus [-k_0, k_0]$$

for the transformed scaled squared energy $\hat{\nu}$ in (3.45).

Provided that the set

$$\begin{aligned}\mathcal{N}_t &:= \left\{ r \in (-k_0, k_0) \setminus \{0\} : \left\langle \nabla \nu_t(r\tilde{\boldsymbol{\phi}}_t), \begin{pmatrix} -\tilde{\phi}_{t,2} \\ \tilde{\phi}_{t,1} \end{pmatrix} \right\rangle \neq 0 \right\} \quad \text{or} \\ \hat{\mathcal{N}}_t &:= \left\{ \hat{r} \in \mathbb{R} \setminus [-k_0, k_0] : \left\langle \nabla \hat{\nu}_t(\hat{r}\tilde{\boldsymbol{\phi}}_t), \begin{pmatrix} -\tilde{\phi}_{t,2} \\ \tilde{\phi}_{t,1} \end{pmatrix} \right\rangle \neq 0 \right\},\end{aligned}$$

respectively, contains at least two elements, we then have that the angular velocity is given by $\boldsymbol{\omega}_t = (\tilde{\rho}_t\tilde{\boldsymbol{\phi}}_t, \tilde{\zeta}_t)^\top$.

If this is the case for all $t \in [0, T]$, then R is given as the unique solution of the linear initial value problem

$$\begin{aligned}R'_t &= R_t W_t, \quad t \in (0, T), \\ R_0 &= I,\end{aligned}\tag{4.9}$$

where the skew-symmetric matrix $W_t \in \mathbb{R}^{3 \times 3}$ is defined by $W_t \mathbf{y} = (\tilde{\rho}_t\tilde{\boldsymbol{\phi}}_t, \tilde{\zeta}_t)^\top \times \mathbf{y}$ for all $\mathbf{y} \in \mathbb{R}^3$.

Proof: From Lemma 4.1 and Lemma 4.2, we find that the uniqueness implies $\boldsymbol{\phi}_t = \tilde{\boldsymbol{\phi}}_t$ and that therefore also

$$\begin{aligned}\tilde{\rho}_t + \frac{r}{k_0 - \sqrt{k_0^2 - r^2}} \tilde{\zeta}_t &= \rho_t + \frac{r}{k_0 - \sqrt{k_0^2 - r^2}} \zeta_t \quad \text{for all } r \in \mathcal{N}_t, \quad \text{or} \\ k_0 \tilde{\rho}_t + \hat{r} \tilde{\zeta}_t &= k_0 \rho_t + \hat{r} \zeta_t \quad \text{for all } \hat{r} \in \hat{\mathcal{N}}_t,\end{aligned}$$

respectively, holds. Since the function $(-k_0, k_0) \setminus \{0\} \rightarrow \mathbb{R} \setminus [-1, 1]$, $r \mapsto \frac{r}{k_0 - \sqrt{k_0^2 - r^2}}$ is bijective, we have $\tilde{\rho}_t = \rho_t$ and $\tilde{\zeta}_t = \zeta_t$ if any of the two equations is satisfied for two different values r or \hat{r} , respectively.

The equation for the rotations R_t then follows directly from the definition (4.1) of the angular velocity. As a linear ordinary differential equation, the initial value problem (4.9) has a unique solution. \square

We remark that, in contrast to the infinitesimal common line method for the ray transform [7], which requires third order derivatives of the data function, we only need first order derivatives of ν in order to reconstruct the angular velocity completely. Furthermore, we can uniquely recover the rotation, whereas for the ray transform there are always two possible solutions corresponding to a reflection in the direction of the imaging wave.

5 Reconstruction of the Translations

So far, we have only considered the computation of the rotations R_t , $t \in [0, T]$, in the motion (2.11), which we could obtain from the absolute values of the Fourier transforms of our measurements m_t , $t \in [0, T]$, that is, from the scaled squared energy ν defined in (3.1).

To recover the translations $\mathbf{d}_t \in \mathbb{R}^3$, we need to use in addition the phase information in our measurements m . Therefore we define the scaled measurement data

$$\begin{aligned}\mu_t: \mathcal{B}_{k_0}^2 &\rightarrow \mathbb{C}, \\ \mathbf{k} \mapsto \mu_t(\mathbf{k}) &:= -i\sqrt{\frac{2}{\pi}} \kappa(\mathbf{k}) e^{-i\kappa(\mathbf{k})r_M} \mathcal{F}^{(2)}[m_t](\mathbf{k}),\end{aligned}\tag{5.1}$$

which according to (2.14) is in terms of the scattering potential f , the rotation $R_t \in \text{SO}(3)$, and the translation $\mathbf{d}_t \in \mathbb{R}^3$ given by

$$\mu_t(\mathbf{k}) = \mathcal{F}[f](R_t \mathbf{h}(\mathbf{k})) e^{-i\langle \mathbf{d}_t, \mathbf{h}(\mathbf{k}) \rangle}.$$

If we have already reconstructed the rotations R_t , then we know (in the case $R_s \mathbf{e}^3 \neq \pm R_t \mathbf{e}^3$) the elliptic arcs $\gamma_{s,t}$ and the dual arcs $\check{\gamma}_{s,t}$ along which the values of the scaled squared energies $\nu_s = |\mu_s|^2$ and $\nu_t = |\mu_t|^2$ coincide as described by (3.17) and (3.29). Therefore, the corresponding values of μ_s and μ_t only differ by a phase factor, which depends on the translation vectors \mathbf{d}_s and \mathbf{d}_t .

Lemma 5.1 *Let $s, t \in [0, T]$ be such that $R_s \mathbf{e}^3 \neq \pm R_t \mathbf{e}^3$ and let $\gamma_{s,t}$ and $\gamma_{t,s}$ be the elliptic arcs defined in Lemma 3.2 and $\sigma_{s,t} = R_s(\mathbf{h} \circ \gamma_{s,t})$ be the corresponding common circular arc introduced in Lemma 3.1. Moreover, let $\check{\gamma}_{s,t}$ and $\check{\gamma}_{t,s}$ be the dual elliptic arcs and $\check{\sigma}_{s,t} = R_s(\mathbf{h} \circ \check{\gamma}_{s,t})$ be the corresponding dual common circular arc as defined in Lemma 3.5.*

(i) *Then we have for every $\beta \in J_{s,t}$ with $\mu_s(\gamma_{s,t}(\beta)) \neq 0$ that*

$$e^{i\langle R_t \mathbf{d}_t - R_s \mathbf{d}_s, \sigma_{s,t}(\beta) \rangle} = \frac{\mu_s(\gamma_{s,t}(\beta))}{\mu_t(\gamma_{t,s}(-\beta))}. \quad (5.2)$$

(ii) *And we have for every $\beta \in \check{J}_{s,t}$ with $\mu_s(\check{\gamma}_{s,t}(\beta)) \neq 0$ that*

$$e^{i\langle R_t \mathbf{d}_t - R_s \mathbf{d}_s, \check{\sigma}_{s,t}(\beta) \rangle} = \frac{\mu_s(\check{\gamma}_{s,t}(\beta))}{\mu_t(\check{\gamma}_{t,s}(\beta))}. \quad (5.3)$$

Proof:

(i) Since the elliptic arcs $\gamma_{s,t}$ and $\gamma_{t,s}$ have by construction the symmetry (3.16), we have for all $\beta \in J_{s,t}$ that

$$\begin{aligned} \mu_s(\gamma_{s,t}(\beta)) &= \mathcal{F}[f](R_s \mathbf{h}(\gamma_{s,t}(\beta))) e^{-i\langle R_s \mathbf{d}_s, R_s \mathbf{h}(\gamma_{s,t}(\beta)) \rangle} \\ &= \mathcal{F}[f](R_t \mathbf{h}(\gamma_{t,s}(-\beta))) e^{-i\langle R_s \mathbf{d}_s, R_t \mathbf{h}(\gamma_{t,s}(-\beta)) \rangle} \\ &= \mu_t(\gamma_{t,s}(-\beta)) e^{i\langle R_t \mathbf{d}_t - R_s \mathbf{d}_s, R_t \mathbf{h}(\gamma_{t,s}(-\beta)) \rangle}, \end{aligned}$$

which implies (5.2) provided that $\mu_s(\gamma_{s,t}(\beta))$ (or, equivalently, $\mu_t(\gamma_{t,s}(-\beta))$) does not vanish.

(ii) In the same way, the elliptic arcs $\check{\gamma}_{s,t}$ and $\check{\gamma}_{t,s}$ have the symmetry (3.28). With the symmetry property (3.20) of $\mathcal{F}[f]$, we get for all $\beta \in \check{J}_{s,t}$ that

$$\begin{aligned} \mu_s(\check{\gamma}_{s,t}(\beta)) &= \mathcal{F}[f](R_s \mathbf{h}(\check{\gamma}_{s,t}(\beta))) e^{-i\langle R_s \mathbf{d}_s, R_s \mathbf{h}(\check{\gamma}_{s,t}(\beta)) \rangle} \\ &= \mathcal{F}[f](-R_t \mathbf{h}(\check{\gamma}_{t,s}(\beta))) e^{i\langle R_s \mathbf{d}_s, R_t \mathbf{h}(\check{\gamma}_{t,s}(\beta)) \rangle} \\ &= \overline{\mu_t(\check{\gamma}_{t,s}(\beta))} e^{i\langle R_s \mathbf{d}_s - R_t \mathbf{d}_t, R_t \mathbf{h}(\check{\gamma}_{t,s}(\beta)) \rangle}, \end{aligned}$$

which implies (5.3) provided that $\mu_s(\check{\gamma}_{s,t}(\beta))$ (or, equivalently, $\mu_t(\check{\gamma}_{t,s}(\beta))$) does not vanish.

□

In the degenerate cases $R_s \mathbf{e}^3 = \pm R_t \mathbf{e}^3$, a similar relation holds on the whole hemisphere.

Lemma 5.2 Let $R_s^\top R_t$ be known for some $s, t \in [0, T]$, and let $\hat{R}^{(3)}$ and S be defined as in (3.30) and (3.32).

(i) If $R_s^\top R_t e^3 = e^3$ and therefore, according to Lemma 3.7, $R_s^\top R_t e^3 = R^{(3)}(\psi)$ for some $\psi \in \mathbb{R}/(2\pi\mathbb{Z})$, then we have for all $\mathbf{k} \in \mathcal{B}_{k_0}^2$ with $\mu_s(\mathbf{k}) \neq 0$

$$e^{i\langle R_t \mathbf{d}_t - R_s \mathbf{d}_s, R_s \mathbf{h}(\mathbf{k}) \rangle} = \frac{\mu_s(\mathbf{k})}{\mu_t(\hat{R}^{(3)}(-\psi)\mathbf{k})}. \quad (5.4)$$

(ii) If $R_s^\top R_t e^3 = -e^3$ and thus, according to Lemma 3.8, $R_s^\top R_t e^3 = R^{(2)}(\pi)R^{(3)}(\psi)$ for some $\psi \in \mathbb{R}/(2\pi\mathbb{Z})$, then we have for all $\mathbf{k} \in \mathcal{B}_{k_0}^2$ with $\mu_s(\mathbf{k}) \neq 0$

$$e^{i\langle R_t \mathbf{d}_t - R_s \mathbf{d}_s, R_s \mathbf{h}(\mathbf{k}) \rangle} = \frac{\mu_s(\mathbf{k})}{\mu_t(\hat{R}^{(3)}(-\psi)S\mathbf{k})}. \quad (5.5)$$

Proof:

(i) If $R_s^\top R_t e^3 = e^3$, we get for all $\mathbf{k} \in \mathcal{B}_{k_0}^2$, using that $R_s \mathbf{h}(\mathbf{k}) = R_t \mathbf{h}(\hat{R}^{(3)}(-\psi)\mathbf{k})$ according to (3.31),

$$\begin{aligned} \mu_t(\hat{R}^{(3)}(-\psi)\mathbf{k}) &= \mathcal{F}[f](R_t \mathbf{h}(\hat{R}^{(3)}(-\psi)\mathbf{k})) e^{-i\langle R_t \mathbf{d}_t, R_t \mathbf{h}(\hat{R}^{(3)}(-\psi)\mathbf{k}) \rangle} \\ &= \mathcal{F}[f](R_s \mathbf{h}(\mathbf{k})) e^{-i\langle R_t \mathbf{d}_t, R_s \mathbf{h}(\mathbf{k}) \rangle} = \mu_s(\mathbf{k}) e^{-i\langle R_t \mathbf{d}_t - R_s \mathbf{d}_s, R_s \mathbf{h}(\mathbf{k}) \rangle}. \end{aligned}$$

(ii) Similarly, we get for all $\mathbf{k} \in \mathcal{B}_{k_0}^2$ in the case $R_s^\top R_t e^3 = -e^3$ with the corresponding relation $-R_s \mathbf{h}(\mathbf{k}) = R_t \mathbf{h}(\hat{R}^{(3)}(-\psi)S\mathbf{k})$ from (3.33) that

$$\begin{aligned} \mu_t(\hat{R}^{(3)}(-\psi)S\mathbf{k}) &= \mathcal{F}[f](R_t \mathbf{h}(\hat{R}^{(3)}(-\psi)S\mathbf{k})) e^{-i\langle R_t \mathbf{d}_t, R_t \mathbf{h}(\hat{R}^{(3)}(-\psi)S\mathbf{k}) \rangle} \\ &= \mathcal{F}[f](-R_s \mathbf{h}(\mathbf{k})) e^{i\langle R_t \mathbf{d}_t, R_s \mathbf{h}(\mathbf{k}) \rangle} = \overline{\mu_s(\mathbf{k})} e^{i\langle R_t \mathbf{d}_t - R_s \mathbf{d}_s, R_s \mathbf{h}(\mathbf{k}) \rangle}. \quad \square \end{aligned}$$

In contrast to data of the ray transform, where the measurements are invariant to the object's position in direction of the incident wave, the diffraction data are not invariant with respect to the third component of the translations, and we can uniquely recover the translation vectors \mathbf{d}_t , $t \in [0, T]$, from the equations (5.2), (5.3), (5.4), and (5.5).

Theorem 5.3 Let the relative rotation $R_s^\top R_t$ be known for some $s, t \in [0, T]$.

(i) If $e^3 \neq \pm R_s^\top R_t e^3$, then the relative translation $R_s^\top R_t \mathbf{d}_t - \mathbf{d}_s$ is uniquely determined from the scaled measurements μ_s and μ_t by the equations (5.2) and (5.3).

(ii) If $e^3 = \pm R_s^\top R_t e^3$, then the relative translation $R_s^\top R_t \mathbf{d}_t - \mathbf{d}_s$ is uniquely determined from the scaled measurements μ_s and μ_t by the equation (5.4) or (5.5), respectively.

Proof:

(i) Since we know from our assumptions on the scattering potential f , see (2.4), that

$$|\mu_s(\mathbf{0})| = |\mathcal{F}[f](\mathbf{0})| = (2\pi)^{-\frac{3}{2}} \int_{\mathbb{R}^3} f(\mathbf{x}) \, d\mathbf{x} > 0,$$

we have that the equations (5.2) and (5.3) hold for all β in some open interval J around 0. By taking the logarithm of these equations, we find with the circular arcs $\boldsymbol{\sigma}_{s,t}$ and $\check{\boldsymbol{\sigma}}_{s,t}$, defined in (3.5) and (3.22), that

$$\langle R_t \mathbf{d}_t - R_s \mathbf{d}_s, \boldsymbol{\sigma}_{s,t}(\beta) \rangle = M(\beta) \quad \text{and} \quad (5.6)$$

$$\langle R_t \mathbf{d}_t - R_s \mathbf{d}_s, \check{\boldsymbol{\sigma}}_{s,t}(\beta) \rangle = \check{M}(\beta) \quad (5.7)$$

for all $\beta \in J$, where the functions $M: J \rightarrow \mathbb{C}$ and $\check{M}: J \rightarrow \mathbb{C}$, given by

$$\begin{aligned} M(\beta) &:= -i \int_0^\beta \frac{F'(\tilde{\beta})}{F(\tilde{\beta})} d\tilde{\beta}, & F(\beta) &:= \frac{\mu_s(\gamma_{s,t}(\beta))}{\mu_t(\gamma_{t,s}(-\beta))}, \quad \text{and} \\ \check{M}(\beta) &:= -i \int_0^\beta \frac{\check{F}'(\tilde{\beta})}{\check{F}(\tilde{\beta})} d\tilde{\beta}, & \check{F}(\beta) &:= \frac{\mu_s(\check{\gamma}_{s,t}(\beta))}{\mu_t(\check{\gamma}_{t,s}(\beta))}, \end{aligned}$$

are explicitly known. Here, we used that the left-hand sides of (5.6) and (5.7) vanish for $\beta = 0$ to choose the correct branch of the logarithm of the continuously differentiable and nowhere vanishing functions F and \check{F} .

Inserting the expressions (3.5) and (3.22) for the circular arcs $\sigma_{s,t}$ and $\check{\sigma}_{s,t}$, respectively, we find, using the notation from Lemma 3.1 and Lemma 3.5, that we have for all $\beta \in J$ the equation system

$$\begin{aligned} a_{s,t}(\cos(\beta) - 1) \langle R_s^\top R_t \mathbf{d}_t - \mathbf{d}_s, R_s^\top \mathbf{v}_{s,t}^1 \rangle + a_{s,t} \sin(\beta) \langle R_s^\top R_t \mathbf{d}_t - \mathbf{d}_s, R_s^\top \mathbf{v}_{s,t}^2 \rangle &= M(\beta), \\ \check{a}_{s,t}(\cos(\beta) - 1) \langle R_s^\top R_t \mathbf{d}_t - \mathbf{d}_s, R_s^\top \mathbf{v}_{s,t}^3 \rangle + \check{a}_{s,t} \sin(\beta) \langle R_s^\top R_t \mathbf{d}_t - \mathbf{d}_s, R_s^\top \mathbf{v}_{s,t}^2 \rangle &= \check{M}(\beta). \end{aligned}$$

Since the functions $\beta \mapsto \cos(\beta) - 1$ and $\beta \mapsto \sin(\beta)$ are linearly independent on every interval with positive length, this implies that the coefficients

$$\langle R_s^\top R_t \mathbf{d}_t - \mathbf{d}_s, R_s^\top \mathbf{v}_{s,t}^j \rangle, \quad j \in \{1, 2, 3\},$$

are uniquely determined by this (recalling that we explicitly know the parameters $a_{s,t} \neq 0$ and $\check{a}_{s,t} \neq 0$). Since $(R_s^\top \mathbf{v}_{s,t}^j)_{j=1}^3$ is an orthonormal basis of \mathbb{R}^3 (which we also know explicitly), this uniquely determines the vector $R_s^\top R_t \mathbf{d}_t - \mathbf{d}_s \in \mathbb{R}^3$.

- (ii) Since $\mu_s(\mathbf{0}) \neq 0$, we find an open disk $A \subset \mathcal{B}_{k_0}^2$ that contains $\mathbf{0}$ such that we have $\mu_s(\mathbf{k}) \neq 0$ for all $\mathbf{k} \in A$. If $R_s^\top R_t \mathbf{e}^3 = \mathbf{e}^3$, we have that $R_s^\top R_t = R^{(3)}(\psi)$ for some $\psi \in \mathbb{R}/(2\pi\mathbb{Z})$ and (5.4) implies

$$\langle R_s^\top R_t \mathbf{d}_t - \mathbf{d}_s, \mathbf{h}(\mathbf{k}) \rangle = -i \int_{C_{\mathbf{0},\mathbf{k}}} \frac{\nabla G(\tilde{\mathbf{k}})}{G(\tilde{\mathbf{k}})} d\tilde{\mathbf{k}} \quad \text{with} \quad G(\mathbf{k}) := \frac{\mu_s(\mathbf{k})}{\mu_t(\hat{R}^{(3)}(-\psi)\mathbf{k})}$$

for all $\mathbf{k} \in A$, where $C_{\mathbf{0},\mathbf{k}}$ denotes an arbitrary curve from $\mathbf{0}$ to \mathbf{k} in A . Since the vectors $\mathbf{h}(\mathbf{k})$ cover for $\mathbf{k} \in A$ an open subset of the hemisphere \mathcal{H}_0 , they span all of \mathbb{R}^3 , and thus this equation uniquely determines the vector $R_s^\top R_t \mathbf{d}_t - \mathbf{d}_s \in \mathbb{R}^3$.

Similarly, we have for $R_s^\top R_t \mathbf{e}^3 = -\mathbf{e}^3$ that $R_s^\top R_t = R^{(2)}(\pi)R^{(3)}(\psi)$ for some $\psi \in \mathbb{R}/(2\pi\mathbb{Z})$ and according to (5.5)

$$\langle R_s^\top R_t \mathbf{d}_t - \mathbf{d}_s, \mathbf{h}(\mathbf{k}) \rangle = -i \int_{C_{\mathbf{0},\mathbf{k}}} \frac{\nabla \check{G}(\tilde{\mathbf{k}})}{\check{G}(\tilde{\mathbf{k}})} d\tilde{\mathbf{k}} \quad \text{with} \quad \check{G}(\mathbf{k}) := \frac{\mu_s(\mathbf{k})}{\mu_t(\hat{R}^{(3)}(-\psi)S\mathbf{k})}$$

for all $\mathbf{k} \in A$, which again uniquely determines $R_s^\top R_t \mathbf{d}_t - \mathbf{d}_s$. \square

Thus, if f is sufficiently irregular so that we find for each $t \in [0, T]$ a time $s \in [0, T]$, for which R_s was already reconstructed (starting from the normalization $R_0 = I$), and such that there either exist unique elliptic arcs in ν_s and ν_t as described in Theorem 3.9, or we have $R_s \mathbf{e}^3 = \pm R_t \mathbf{e}^3$ and there exists a unique angle ψ fulfilling either (3.30) or (3.32), then Lemma 3.7, Lemma 3.8, and Theorem 3.9 determine uniquely the rotation R_t . And with this knowledge, we get from Theorem 5.3 with $\mathbf{d}_0 = \mathbf{0}$ all the translations \mathbf{d}_t , $t \in [0, T]$, and therefore the complete motion Ψ of our object, introduced in (2.11).

Remark 5.4 We can also detect the optical center $\mathcal{C} \in \mathbb{R}^3$ of the object, that is, the ratio

$$\mathcal{C} := \frac{\int_{\mathbb{R}^3} \mathbf{x} f(\mathbf{x}) \, d\mathbf{x}}{\int_{\mathbb{R}^3} f(\mathbf{x}) \, d\mathbf{x}} = \frac{i \nabla \mathcal{F}[f](\mathbf{0})}{\mathcal{F}[f](\mathbf{0})}$$

of the first and the zeroth moment of the function f , from the data μ by realising that

$$\frac{i \partial_{k_i} \mu_t(\mathbf{0})}{\mu_t(\mathbf{0})} = \frac{i \langle \nabla \mathcal{F}[f](\mathbf{0}), R_t \mathbf{e}^i \rangle}{\mathcal{F}[f](\mathbf{0})} + d_{t,i} = \langle \mathcal{C}, R_t \mathbf{e}^i \rangle + d_{t,i}, \quad i \in \{1, 2\}.$$

If we have a time $t \in [0, T]$ for which the rotation R_t has a rotation axis different from $\mathbb{R} \mathbf{e}^3$, this allows us (other than from data of the ray transform) to fully recover the point $\mathcal{C} \in \mathbb{R}^3$ without the need of first reconstructing f .

Theoretically, this approach also provides a reconstruction of arbitrary moments of the function f by incorporating higher-order derivatives of μ_t , which was used in [20] to prove the unique reconstructability of f . \square

6 Reconstruction Algorithms and Numerical Simulations

We perform numerical tests of the reconstruction algorithms. We compare the approaches of Section 3 and 4 for the case that the motion depends smoothly on time. We consider two three-dimensional test functions for the scattering potential f , namely a cell phantom in Figure 7a, which consists of different convex and concave shapes with constant function values, and the Shepp–Logan phantom in Figure 7b. Both are evaluated on a uniform $N \times N \times N$ grid with $N = 160$ and they are not rotationally symmetric. Otherwise, any symmetry would cause the motion detection to have multiple solutions.

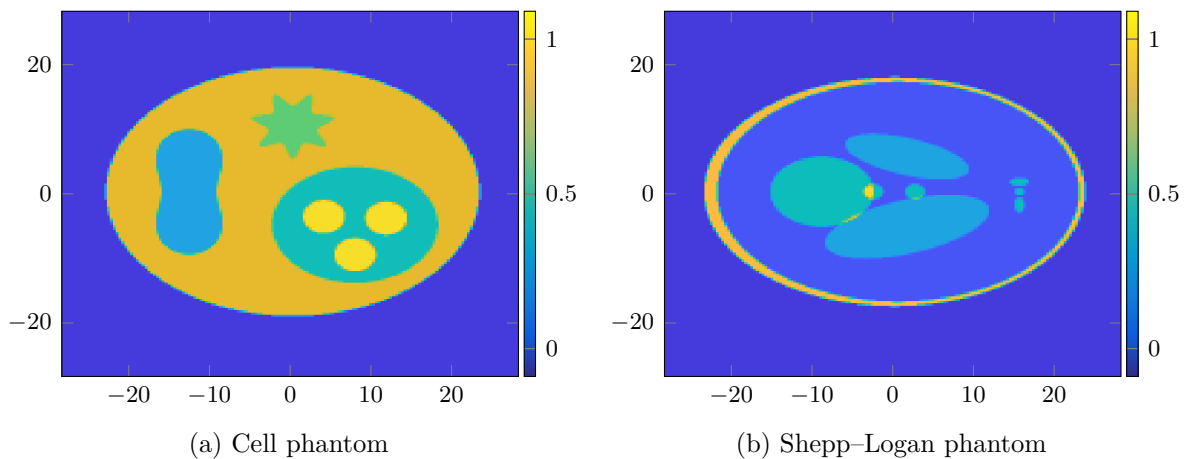


Figure 7: Slice plots the 3D phantoms f at $x_3 = 0$.

The data ν_t is computed “in silico” via a numerical approximation of the Fourier transform $\mathcal{F}[f]$, where f is discretized on a finer grid of $(3N)^3 \approx 1.1 \cdot 10^8$ points. This approximation is done with the nonuniform fast Fourier transform (NFFT) algorithm [31], the same way as in [19]. We evaluate ν_t on a polar grid $(r \cos(\alpha), r \sin(\alpha))^T$ on $\mathcal{B}_{k_0}^2$ consisting of $2N$ points in $r \in (-k_0, k_0)$ and $2N$ points of $\alpha \in [0, \pi)$. We set the wave number $k_0 = 2\pi$, which corresponds to a wavelength of one of the incident wave. Furthermore, we have $4N = 640$ equispaced samples of the time $t \in [0, 2\pi)$. The high number of grid points yields in a good numerical approximation of the time-derivative. In total, we sample ν on about 65 million data points. We first consider the case that the object is only rotated, but not translated.

Remark 6.1 If the object rotates around the origin without any further translation, i.e., $\mathbf{d}_t = \mathbf{0}$ for all t , then the function ν_t used for the common circle and infinitesimal common circle methods, see [Section 3](#) and [Section 4](#), can be everywhere replaced by the complex-valued function μ_t from [\(5.1\)](#), since then the exponent in the phase factors in [\(2.14\)](#) vanishes. We make use of this in our first numerical tests. \square

Reconstruction of the angular velocity We apply the infinitesimal common circle method of [Section 4](#) for the reconstruction of the angular velocity $\boldsymbol{\omega}_t = (\rho_t \cos(\phi_t), \rho_t \sin(\phi_t), \zeta_t)^\top$, $\rho_t, \zeta_t \in \mathbb{R}$, $\phi_t \in [0, \pi)$, by using that $\boldsymbol{\omega}_t$ fulfills the equation [\(4.5\)](#).

For $r \in (-k_0, k_0)$ and $t \in (0, T)$, we set

$$\begin{aligned} g_{t, \tilde{\phi}}(r) &:= \partial_t \nu_t(r \cos(\tilde{\phi}), r \sin(\tilde{\phi})), \\ p_{t, \tilde{\phi}}(r) &:= \left(k_0 - \sqrt{k_0^2 - r^2} \right) \left\langle \nabla \nu_t(r \cos(\tilde{\phi}), r \sin(\tilde{\phi})), \begin{pmatrix} -\sin(\tilde{\phi}) \\ \cos(\tilde{\phi}) \end{pmatrix} \right\rangle, \\ q_{t, \tilde{\phi}}(r) &:= r \left\langle \nabla \nu_t(r \cos(\tilde{\phi}), r \sin(\tilde{\phi})), \begin{pmatrix} -\sin(\tilde{\phi}) \\ \cos(\tilde{\phi}) \end{pmatrix} \right\rangle. \end{aligned} \quad (6.1)$$

Note that these functions are indeed continuous and they are obtained by differentiating the scaled squared energy ν , which we approximate numerically by central differences on the polar grid. Then relation [\(4.5\)](#) of the angular velocity can be written as

$$g_{t, \phi_t}(r) = \rho_t p_{t, \phi_t}(r) + \zeta_t q_{t, \phi_t}(r), \quad r \in (-k_0, k_0). \quad (6.2)$$

When working with measured data, it is unlikely that [\(6.2\)](#) holds exactly, therefore we make the following least-squares approach in order to recover the quantities ρ_t , ϕ_t and ζ_t . We want to minimize for fixed $t \in (0, T)$ the functional

$$\mathcal{J}_t(\tilde{\rho}, \tilde{\phi}, \tilde{\zeta}) := \left\| g_{t, \tilde{\phi}} - \tilde{\rho} p_{t, \tilde{\phi}} - \tilde{\zeta} q_{t, \tilde{\phi}} \right\|_{L^2(-k_0, k_0)}^2, \quad \tilde{\rho}, \tilde{\zeta} \in \mathbb{R}, \tilde{\phi} \in [0, \pi), \quad (6.3)$$

which vanishes according to [\(6.2\)](#) for $(\tilde{\rho}, \tilde{\phi}, \tilde{\zeta}) = (\rho_t, \phi_t, \zeta_t)$, so that the desired angular velocity $\boldsymbol{\omega}_t$ is indeed a minimizer of \mathcal{J}_t .

We minimize \mathcal{J}_t for fixed $t \in (0, T)$ by a brute-force method. For every $\tilde{\phi} \in [0, \pi)$ on a fixed grid, we compute the minimizer of the functional $\mathcal{J}_{t, \tilde{\phi}}: \mathbb{R}^2 \rightarrow \mathbb{R}$, $\mathcal{J}_{t, \tilde{\phi}}(\tilde{\rho}, \tilde{\zeta}) := \mathcal{J}_t(\tilde{\rho}, \tilde{\phi}, \tilde{\zeta})$, which we can explicitly get from the optimality condition

$$\mathbf{0} = \nabla \mathcal{J}_{t, \tilde{\phi}}(\tilde{\rho}, \tilde{\zeta}) = \begin{pmatrix} \frac{\partial}{\partial \tilde{\rho}} \mathcal{J}_{t, \tilde{\phi}}(\tilde{\rho}, \tilde{\zeta}) \\ \frac{\partial}{\partial \tilde{\zeta}} \mathcal{J}_{t, \tilde{\phi}}(\tilde{\rho}, \tilde{\zeta}) \end{pmatrix} = 2 \begin{pmatrix} \tilde{\rho} \left\langle p_{t, \tilde{\phi}}, p_{t, \tilde{\phi}} \right\rangle - \left\langle g_{t, \tilde{\phi}}, p_{t, \tilde{\phi}} \right\rangle + \tilde{\zeta} \left\langle p_{t, \tilde{\phi}}, q_{t, \tilde{\phi}} \right\rangle \\ \tilde{\zeta} \left\langle q_{t, \tilde{\phi}}, q_{t, \tilde{\phi}} \right\rangle - \left\langle g_{t, \tilde{\phi}}, q_{t, \tilde{\phi}} \right\rangle + \tilde{\rho} \left\langle p_{t, \tilde{\phi}}, q_{t, \tilde{\phi}} \right\rangle \end{pmatrix},$$

where $\langle \cdot, \cdot \rangle$ denotes the inner product on $L^2((-k_0, k_0) \rightarrow \mathbb{R})$ here. Provided that the functions $p_{t, \tilde{\phi}}$ and $q_{t, \tilde{\phi}}$ are linearly independent in $L^2((-k_0, k_0) \rightarrow \mathbb{R})$, so that $\|p\|_{L^2} \|q\|_{L^2} \neq |\langle p, q \rangle|$ as the Cauchy–Schwarz inequality holds with equality if and only if the functions are linearly dependent, this has a unique solution and the unique minimizer $(\tilde{\rho}_{t, \tilde{\phi}}^*, \tilde{\zeta}_{t, \tilde{\phi}}^*)$ is then given by

$$\begin{pmatrix} \tilde{\rho}_{t, \tilde{\phi}}^* \\ \tilde{\zeta}_{t, \tilde{\phi}}^* \end{pmatrix} = \begin{pmatrix} \left\langle p_{t, \tilde{\phi}}, p_{t, \tilde{\phi}} \right\rangle & \left\langle p_{t, \tilde{\phi}}, q_{t, \tilde{\phi}} \right\rangle \\ \left\langle p_{t, \tilde{\phi}}, q_{t, \tilde{\phi}} \right\rangle & \left\langle q_{t, \tilde{\phi}}, q_{t, \tilde{\phi}} \right\rangle \end{pmatrix}^{-1} \begin{pmatrix} \left\langle g_{t, \tilde{\phi}}, p_{t, \tilde{\phi}} \right\rangle \\ \left\langle g_{t, \tilde{\phi}}, q_{t, \tilde{\phi}} \right\rangle \end{pmatrix}.$$

For every $\tilde{\phi} \in [0, \pi)$ on the uniform grid, we thus first calculate the value

$$j_t(\tilde{\phi}) := \min_{\tilde{\rho}, \tilde{\zeta} \in \mathbb{R}} \mathcal{J}_t(\tilde{\rho}, \tilde{\phi}, \tilde{\zeta}) = \mathcal{J}_t(\tilde{\rho}_{t, \tilde{\phi}}^*, \tilde{\phi}, \tilde{\zeta}_{t, \tilde{\phi}}^*), \quad (6.4)$$

then we take as approximation of the angle ϕ_t in the angular velocity $\boldsymbol{\omega}_t$ the minimizer $\tilde{\phi}_t^* \in [0, \pi)$ of j_t on this grid, and pick the minimizers $\tilde{\rho}_{t, \tilde{\phi}_t^*}^*$ and $\tilde{\zeta}_{t, \tilde{\phi}_t^*}^*$ as approximations for ρ_t and ζ_t .

Remark 6.2 The minimizer of \mathcal{J}_t might not be unique in general, depending on the symmetry of the scattering potential f . If, e.g., f is the characteristic function of a unit ball, then ν_t does not depend on t and hence \mathcal{J}_t vanishes everywhere. In the described method, there are two steps of possible non-uniqueness: Firstly, the functions $p_{t,\tilde{\phi}}$ and $q_{t,\tilde{\phi}}$ might be linearly dependent, then the minimizer of $\mathcal{J}_{t,\tilde{\phi}}$ is not unique. Secondly, the subsequent minimization over $\tilde{\phi} \in [0, \pi)$ might lead to more than one minimum point. However, in our numerical tests with non-symmetric functions f , we always computed approximately the right minima, see Figure 8. \square

Let $\mathbb{S}^2 := \{\mathbf{x} \in \mathbb{R}^3 : \|\mathbf{x}\| = 1\}$ denote the two-dimensional sphere. We first consider a constant rotation axis $\mathbf{n} \in \mathbb{S}^2$ and the rotation angle $\alpha(t) = t$, $t \in [0, 2\pi]$, that is, $R(t) = \exp(tN)$ with $N \in \mathbb{R}^{3 \times 3}$ defined by $N\mathbf{x} = \mathbf{n} \times \mathbf{x}$ for all $\mathbf{x} \in \mathbb{R}^3$, since we then have, according to Rodrigues' rotation formula, $R(t)\mathbf{x} = \langle \mathbf{n}, \mathbf{x} \rangle \mathbf{n} + \sin(t)\mathbf{n} \times \mathbf{x} + \cos(t)(\mathbf{n} \times \mathbf{x}) \times \mathbf{n}$ for all $\mathbf{x} \in \mathbb{R}^3$. The angular velocity is in this case therefore the constant function $\boldsymbol{\omega}_t = \mathbf{n}$. In Figure 8, we show the misfit functional j_t for the rotation axis $\mathbf{n} = (0.96 \cos(\pi/4), 0.96 \sin(\pi/4), 0.28)^\top$ at the time $t = \pi/4$. One can clearly spot the expected minimum of j_t at $\tilde{\phi} = \pi/4$. Furthermore, we show the error of the reconstructed angular velocity using the infinitesimal common circle method for all time steps t in Figure 9. We note that the radius ρ_t has a higher error than the other components.

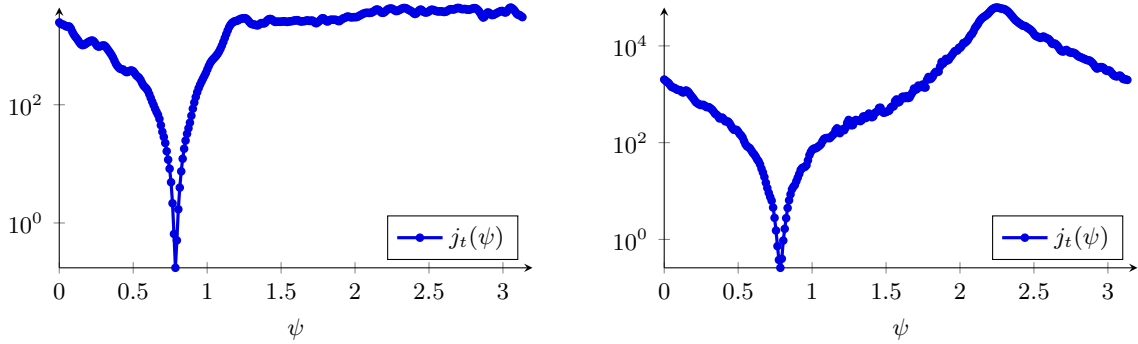


Figure 8: Plot of the function j_t for time step $t = \pi/4$. *Left*: cell phantom, *right*: Shepp–Logan.

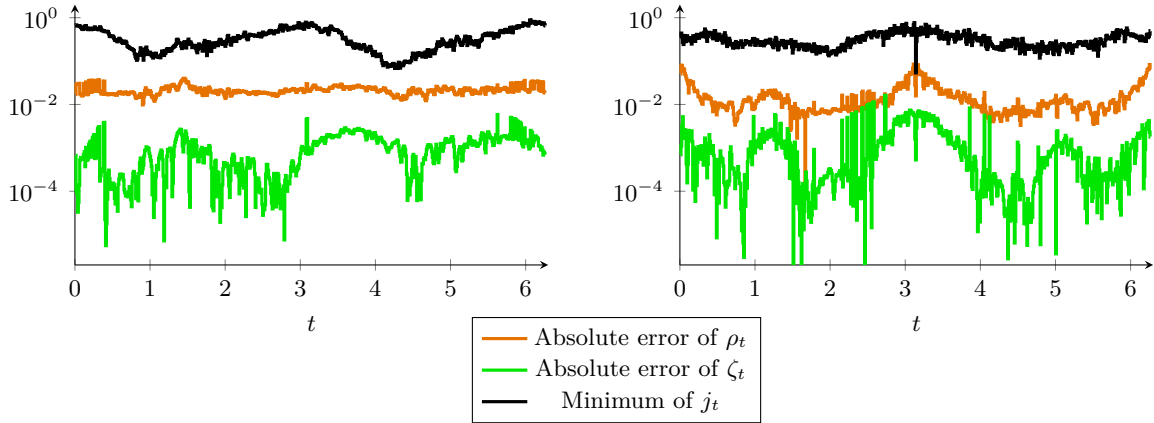


Figure 9: Absolute error of the components (4.2) of the angular velocity $\boldsymbol{\omega}_t$ and the minimum of the functional j_t , depending on t . The reconstructed value for ϕ_t takes only values on the grid, and in this case it is reconstructed exactly; note that the true value is also on the grid. *Left*: cell phantom, *right*: Shepp–Logan phantom.

Remark 6.3 (Sampling) Here, we assume that ν_t is given on a polar grid in order to easily compute the derivatives in (6.1). However, the numerical reconstruction of f for known rotations seems to be a little worse than with a uniform, rectangular grid for ν_t as considered in [19]. However, the actual experiment takes measurements of the scattered wave u_t . Then ν_t is related

to u_t via a 2D Fourier transform in (3.1). It seems natural that the images of u_t are captured on a uniform grid. A canonical discretization of (3.1) is the fast Fourier transform, which gives an approximation of ν_t on a uniform grid, cf. [2]. Nevertheless, the nonuniform fast Fourier transform [27, Section 7] can be used to evaluate ν_t accurately on any set such as a polar grid. \square

Reconstruction of the rotation matrix Next we compute rotation matrices R_t from the given angular velocities ω_t , $t \in (0, T)$. Let us assume the slightly higher regularity $R \in C^2([0, T] \rightarrow \text{SO}(3))$. According to Theorem 4.3, we can obtain R from the angular velocity ω with the corresponding coefficient matrix W by solving the initial value problem (4.9) for $R_t \in \text{SO}(3)$. The Lie group $\text{SO}(3)$ has the Lie algebra $\mathfrak{so}(3)$ consisting of the skew-symmetric 3×3 matrices. As $W_t \in \mathfrak{so}(3)$ for every t , (4.9) has a unique solution in $\text{SO}(3)$ by [10, Section IV.4].

Numerically, the initial value problem (4.9) can be solved with the forward *Euler method* on $\mathbb{R}^{3 \times 3}$ followed by a so-called *retraction* $P_{\tilde{R}}$, see [1], which maps the tangential vectors from the tangent space $\{\tilde{R}\tilde{W} : \tilde{W} \in \mathfrak{so}(3)\}$ at $\tilde{R} \in \text{SO}(3)$ to $\text{SO}(3)$, in each iteration step. More precisely, using discrete time steps $t_j := j/n$ of resolution $n \in \mathbb{N}$, we compute for $j = 1, \dots, \lfloor Tn \rfloor$,

$$\begin{aligned} R_0 &:= I, \\ R_{j+1} &:= P_{R_j}((t_{j+1} - t_j) R_j W_{t_j}). \end{aligned} \tag{6.5}$$

Since the manifold $\text{SO}(3)$ is smooth and $R \in C^2([0, T] \rightarrow \text{SO}(3))$, it is known that this method converges with the same order as the classical Euler method, see [10, Section IV.4].

Several retractions, that are computations of P_{R_j} , are possible in (6.5), see [1, Example 1.4.2], and we state two popular ones in the following. Indeed, their performance is very similar in our numerical computations. If a large number of computations is necessary, e.g., when training neural networks, the chosen method influences the computational time substantially, see [11].

- (i) **Polar decomposition:** Starting with the singular value decomposition $A = U\Sigma V^\top$ of a matrix $A \in \mathbb{R}^{3 \times 3}$ with diagonal matrix Σ and orthogonal matrices U and V , its polar decomposition is given by $A = \text{Polar}(A)\hat{\Sigma}$, where $\text{Polar}(A) := UV^\top$ and $\hat{\Sigma} := V\Sigma V^\top$. If $\det A > 0$, then $\text{Polar}(A) \in \text{SO}(3)$. It is well-known, see, e.g., [24], that $\text{Polar}(A)$ is the orthogonal projection of A onto $\text{SO}(3)$ with respect to the Frobenius norm $\|\cdot\|_F$, i.e.,

$$\text{Polar}(A) = \operatorname{argmin}_{Q \in \text{SO}(3)} \|A - Q\|_F. \tag{6.6}$$

Hence a retraction is given by $P_{\tilde{R}}(\tilde{W}) = \text{Polar}(\tilde{R} + \tilde{W})$.

- (ii) **Cayley transform:** The *Cayley transform*, maps a skew-symmetric matrix $\tilde{W} \in \mathbb{R}^{3 \times 3}$ to

$$\text{Cay}(\tilde{W}) := \left(I - \frac{1}{2}\tilde{W}\right)^{-1} \left(I + \frac{1}{2}\tilde{W}\right) \tag{6.7}$$

and then a retraction is given by $P_{\tilde{R}}(\tilde{W}) = \tilde{R} \text{Cay}(\tilde{W})$.

For the rotation of a full turn, we use Euler's method in (6.5). The reconstructions are denoted as R_t^{Pol} with the polar decomposition (6.6), and R_t^{Cay} with the Cayley transform (6.7) as retraction. The resulting error, measured in the Frobenius norm, is shown in Figure 10, where we see that the reconstructions with both retractions perform almost equally.

Combination of the infinitesimal with the regular common circle method The error of the reconstruction in Figure 10 based on Euler's method grows with the time t . This behavior is quite expected since we make a small error in each time step and the errors accumulate.

One way of compensating for this consists in combining this reconstruction based on the infinitesimal approach with the common circle method of [Section 3](#) for directly finding the common circles.

To this end, we use the explicit parametrization (3.19) of the elliptic arc $\gamma_{s,t}$ and try to find the Euler angles $(\varphi, \theta, \psi) \in (\mathbb{R}/(2\pi\mathbb{Z})) \times [0, \pi] \times (\mathbb{R}/(2\pi\mathbb{Z}))$ of the rotation $R_s^\top R_t$ by solving $\nu_s(\gamma_{s,t}(\beta)) = \nu_t(\gamma_{t,s}(-\beta))$ for all $\beta \in J_{s,t}$ as described in [Theorem 3.9](#). We again formulate this as a least-squares minimization problem, which leads us to the functional

$$\mathcal{E}_{s,t}(\tilde{\varphi}, \tilde{\theta}, \tilde{\psi}) := \int_{-c(\tilde{\theta})}^{c(\tilde{\theta})} \left| \nu_t(\gamma^{\pi-\tilde{\psi}, \tilde{\theta}}(-\beta)) - \nu_s(\gamma^{\tilde{\varphi}, \tilde{\theta}}(\beta)) \right|^2 d\beta, \quad \tilde{\varphi}, \tilde{\psi} \in \mathbb{R}/(2\pi\mathbb{Z}), \tilde{\theta} \in [0, \pi], \quad (6.8)$$

where we write the elliptic arc $\gamma_{s,t}$ as a function of the Euler angles,

$$\gamma^{\tilde{\varphi}, \tilde{\theta}}(\beta) := \frac{k_0}{2} \sin(\tilde{\theta})(\cos(\beta) - 1) \begin{pmatrix} \cos(\tilde{\varphi}) \\ \sin(\tilde{\varphi}) \end{pmatrix} + k_0 \cos(\frac{\tilde{\theta}}{2}) \sin(\beta) \begin{pmatrix} -\sin(\tilde{\varphi}) \\ \cos(\tilde{\varphi}) \end{pmatrix},$$

see (3.19), and use the function c to parametrize the interval $J_{s,t}$, defined in (3.7), by setting $c(\tilde{\theta}) := \arccos(\frac{\cos(\tilde{\theta})-1}{\cos(\tilde{\theta})+1})$ for $\tilde{\theta} \in [0, \frac{\pi}{2}]$ and $c(\tilde{\theta}) := \pi$ for $\tilde{\theta} \in (\frac{\pi}{2}, \pi]$. We then consider the minimizer of $\mathcal{E}_{s,t}$ as a good approximation of the Euler angles (φ, θ, ψ) of the rotation $R_s^\top R_t$.

The minimization of $\mathcal{E}_{s,t}$ is a three-dimensional, non-linear and non-convex optimization problem. However, the computation of the minimum of (6.8) becomes much more efficient if we have a good starting curve at hand. We therefore start with the solution obtained with the infinitesimal method, which already is a good starting solution R_t^{Cay} for the minimization of $\mathcal{E}_{s,t}$. We perform the latter using the Nelder–Mead downhill simplex method [22], which does not require derivatives and is implemented in Matlab's `fminsearch` routine. The evaluation of the data ν_t , which is available on a polar grid, at the curves $\gamma^{\tilde{\varphi}, \tilde{\theta}}$ is utilizing cubic interpolation.

The error of the reconstruction with this combined approach is shown in [Figure 10](#). We see that the reconstruction greatly benefits from the combined approach.

Furthermore, we have noticed that taking a random starting solution for the optimization of (6.8) often yields very bad results, since $\mathcal{E}_{s,t}$ might have multiple local minima. A possible approach would consist in evaluating $\mathcal{E}_{s,t}$ on a grid in \mathbb{R}^3 and taking the minimum or by using multiple random starting solutions. However, this seems unnecessary, since we can rely on the good starting solution obtained with the infinitesimal method.

Reconstruction with moving rotation axis In our next simulation, we consider the time-dependent rotation axis $\mathbf{n}(t) = (\sqrt{1-a^2} \cos(b \sin(t/2)), \sqrt{1-a^2} \sin(b \sin(t/2)), a)^\top \in \mathbb{S}^2$ for $a = 0.28$ and $b = 0.5$. The obtained error is shown in [Figure 11](#). Overall, the results are similar to the ones for the constant rotation axis. However, there is a larger error around $t \approx 0$. This might be explained by the fact that for a small rotation the respective hemispheres and thus also the data ν_t and ν_0 are very close together, which makes detecting the common circles harder. This could be circumvented by applying the common circles method to rotations that are farther apart. A similar observation was made that the common lines in context of the ray transform also become harder to detect in case of very small rotations where the infinitesimal method suits better, see [7].

Reconstruction of the translation Now, we consider the case that the object also moves according to the translation $\mathbf{d}_t = 4(\sin t, \sin t, \sin t)^\top$, $t \in [0, 2\pi]$, and the rotation is the same as in the previous example with the moving axis. We first reconstruct the rotations with the

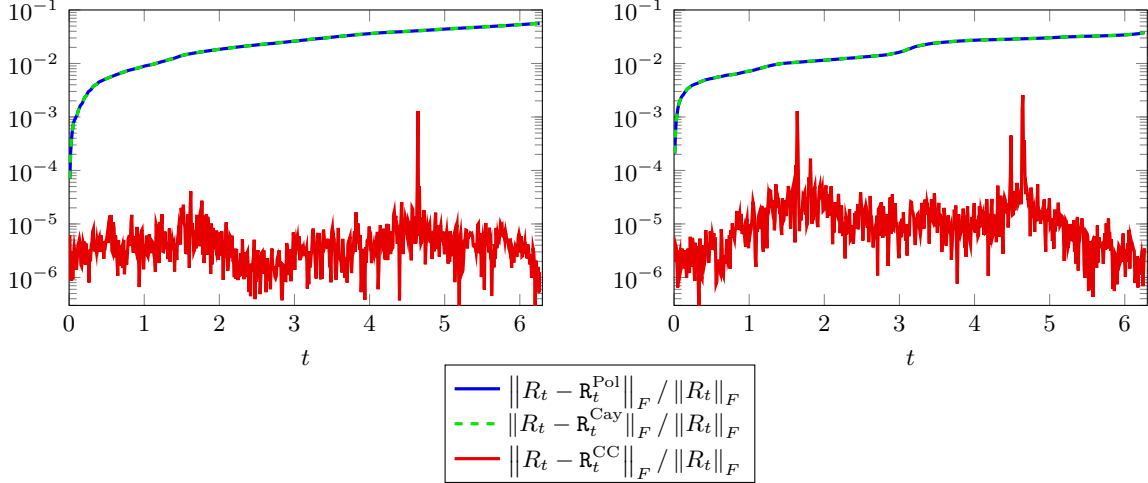


Figure 10: Relative error of the reconstructed rotation matrices R_t^{Pol} and R_t^{Cay} using Euler's method (6.5) with the polar decomposition (6.6) or the Cayley transform (6.7), respectively. Furthermore, R_t^{CC} refers to the rotation matrix reconstructed with the minimization of (6.8) to find the common circles, where the starting solution of the optimization was in each step computed with the infinitesimal method and the Cayley transform as above. *Left*: cell phantom, *right*: Shepp-Logan phantom.

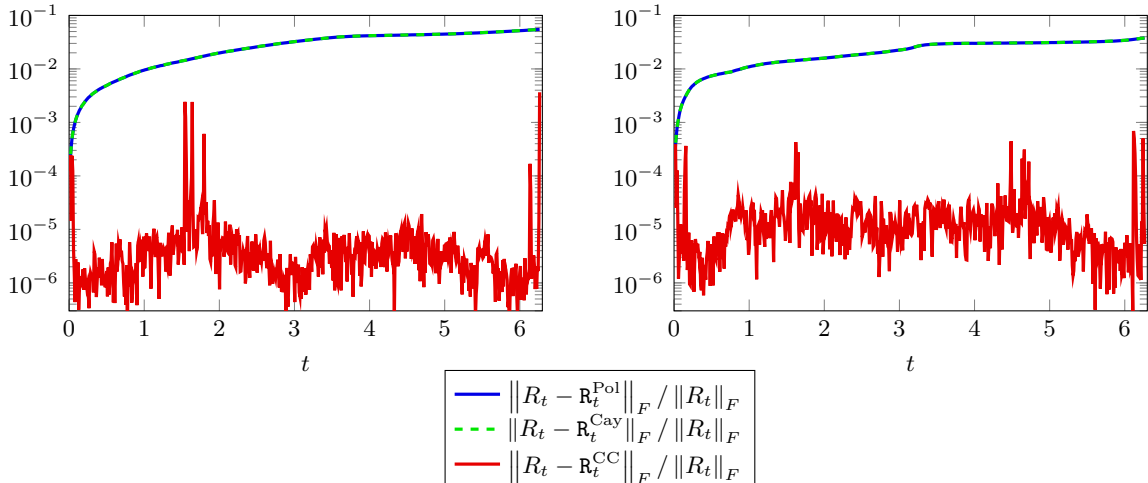


Figure 11: Relative error of the rotation matrix R_t , reconstructed using the same setup and methods as in Figure 10, but with a moving rotation axis.

same methods as above, using the real-valued function ν_t of (3.1). Afterwards, we recover the translations as in Theorem 5.3 from the nonlinear equations (5.2) and (5.3) for some $s, t \in [0, T]$ with the following approach.

The left-hand side of (5.2) is continuous with respect to β , and the term $\sigma_{s,t}(\beta)$ in its exponent vanishes for $\beta = 0$. We can compute the minimum norm least-squares solution $\mathbf{d}_{t;s} \in \mathbb{R}^3$ of the linear system

$$\langle \mathbf{d}_{t;s}, \sigma_{s,t}(\beta) \rangle = \text{unwrap} \left(\frac{1}{i} \log \left(\frac{\mu_s(\gamma_{s,t}(\beta))}{\mu_t(\gamma_{t,s}(-\beta))} \right) \right), \quad \beta \in J, \quad (6.9)$$

where unwrap denotes a phase unwrapping [12] that vanishes at $\beta = 0$ and J is an interval around 0 on which $\mu_s \circ \gamma_{s,t}$ is nowhere zero. For reconstructing the translation \mathbf{d}_t , we take

the minimum norm solution fulfilling both (6.9), which is obtained from (5.2), as well as the analogous relation obtained from (5.3). Especially for large translations, we have noted in the simulations that the unwrapping does not always yield good results because of the inexactness of the data. This could be mitigated by combining it with a nonlinear optimization directly applied to (5.2) and (5.3).

The reconstruction error is shown in Figure 12, where we see that the translation is reconstructed quite reliably. The error of the rotation is larger than in the case without translation, but it is still on an acceptable level. Note that we can only use the absolute value data ν_t for reconstructing the rotations if the translations do not vanish, cf. Remark 6.1.

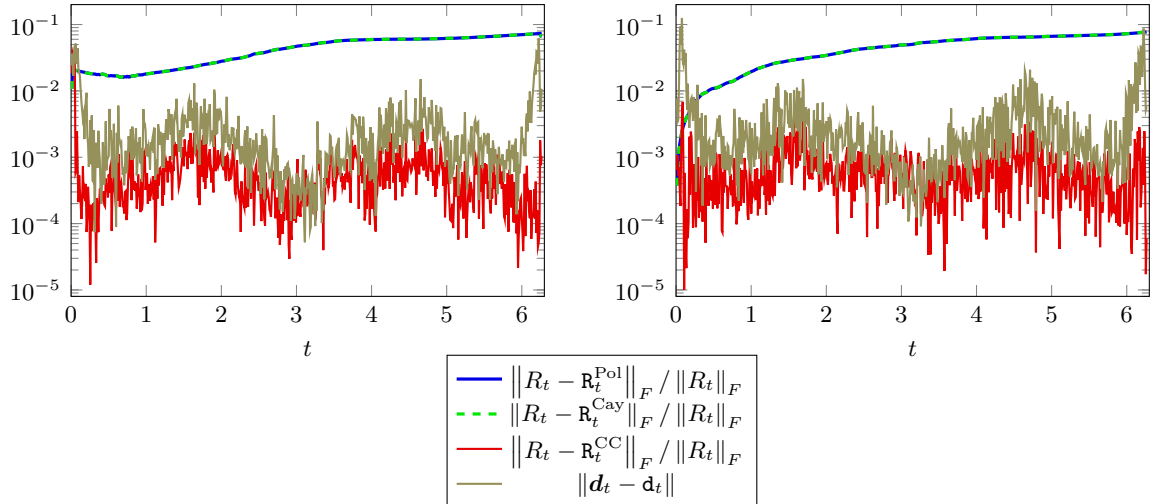


Figure 12: Error of the reconstructed rotation matrix and reconstructed translation \mathbf{d}_t , for the case of a non-zero translation. Note that $\|\mathbf{d}_t\|$ varies between 0 and approximately 6.9, so it does not make sense to compute relative errors. *Left*: cell phantom, *Right*: Shepp–Logan phantom.

Finally, we show in Figure 13 the reconstructed images of the scattering potential f , where we have first computed the rotations and translations with the above combined common circle method for the moving rotation axis. In the second part, i.e., the image reconstruction with known motion, we use the nonuniform Fourier reconstruction technique from [19]. For the image reconstruction, we evaluate μ_t on a uniform grid instead of the polar grid used for the common circle method, since the reconstruction of the image f for a polar grid shows an inferior quality. This observation is consistent with numerical evidence in [9], which showed that an approximate inversion of discrete Fourier transforms on a two-dimensional polar grid often shows large errors even for a very large number of sampling points.

Computational time The numerical simulations were performed with Matlab on a standard PC with an 8-core Intel i7-10700 processor and 32 GB of memory. We utilized the NFFT software package [17, 16] for the Fourier transforms. The reconstruction of the motion parameters for all 640 time steps as in Figure 12 took about 40 seconds. The image reconstruction in Figure 13 took about 90 seconds.

7 Conclusions

In this paper, we have considered the reconstruction of the motion of an object in diffraction tomography. For the reconstruction of the rotation, we have presented a common circle method and its infinitesimal version. While the former method usually produced more accurate results, it benefits from using a starting solution with the computationally faster infinitesimal approach.

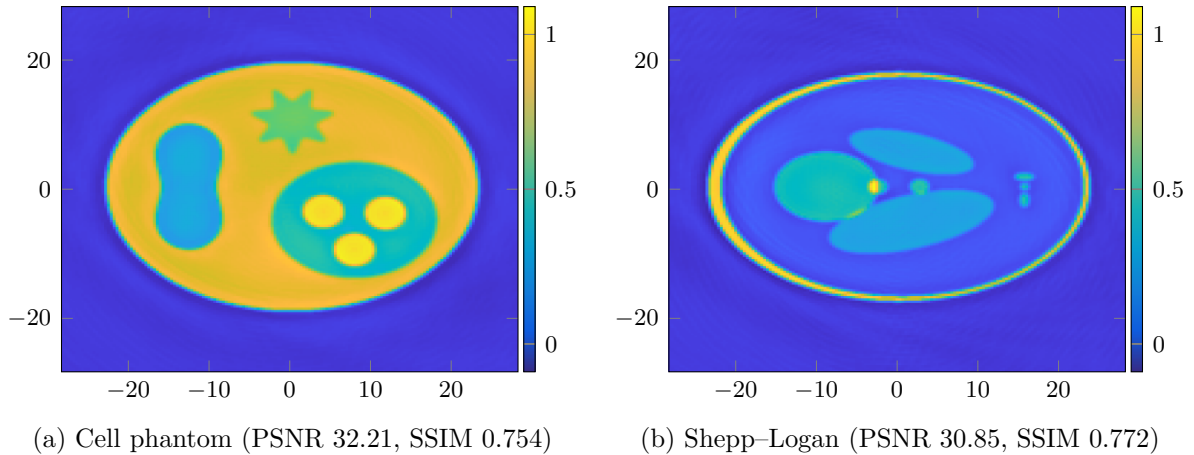


Figure 13: Slice plots of the reconstructed scattering potential f , where the rotation and translation was estimated with the common circle method as in Figure 12. The image quality is assessed via the peak signal-to-noise ratio (PSNR) and the structural similarity index (SSIM).

Furthermore, we have shown that also the translation of the object can be uniquely recovered from the diffraction data. For this, we have required that the scattering potential is real-valued. We note that, in contrast to projection images corresponding to the ray transform, also the position and orientation of the object in direction of the incident wave can be detected here.

Future research will focus on the real-world application related to optical diffraction tomography with acoustical tweezers. Furthermore, we intend to incorporate phase retrieval methods for the motion detection since often only the intensities of the field $u^{\text{sca}} + u^{\text{inc}}$ can be measured.

Acknowledgments

Funding by the DFG under the SFB “Tomography Across the Scales” (STE 571/19-1, project number: 495365311) is gratefully acknowledged. Moreover, PE and OS are supported by the Austrian Science Fund (FWF), with SFB F68 “Tomography Across the Scales”, project F6804-N36 and F6807-N36. The financial support by the Austrian Federal Ministry for Digital and Economic Affairs, the National Foundation for Research, Technology and Development and the Christian Doppler Research Association is gratefully acknowledged. This research was funded in whole, or in part, by the Austrian Science Fund (FWF) P 34981. For the purpose of open access, the authors have applied a CC BY public copyright license to any Authors Accepted Manuscript version arising from this submission.

References

- [1] P.-A. Absil, R. Mahony, and R. Sepulchre. *Optimization Algorithms on Matrix Manifolds*. Princeton University Press, 2008.
- [2] R. Beinert and M. Quellmalz. Total variation-based reconstruction and phase retrieval for diffraction tomography. *SIAM Journal on Imaging Sciences*, 15(3):1373–1399, 2022.
- [3] T. Bendory, A. Bartesaghi, and A. Singer. Single-particle cryo-electron microscopy: Mathematical theory, computational challenges, and opportunities. *IEEE Signal Processing Magazine*, 37(2):58–76, 2020.

- [4] D. Colton and R. Kress. *Inverse Acoustic and Electromagnetic Scattering Theory*. Number 93 in Applied Mathematical Sciences. Springer, Berlin, 3rd edition, 2013.
- [5] A. Devaney. A filtered backpropagation algorithm for diffraction tomography. *Ultrasonic Imaging*, 4(4):336–350, 1982.
- [6] K. Dholakia, B. W. Drinkwater, and M. Ritsch-Marte. Comparing acoustic and optical forces for biomedical research. *Nature Reviews Physics*, 2(9):480–491, 2020.
- [7] P. Elbau, M. Ritsch-Marte, O. Scherzer, and D. Schmutz. Motion reconstruction for optical tomography of trapped objects. *Inverse Problems*, 36(4):044004, 2020.
- [8] F. Faucher, C. Kirisits, M. Quellmalz, O. Scherzer, and E. Setterqvist. Diffraction tomography, Fourier reconstruction, and full waveform inversion. *ArXiv 2110.07921*, 2021.
- [9] M. Fenn, S. Kunis, and D. Potts. On the computation of the polar FFT. *Applied and Computational Harmonic Analysis*, 22:257–263, 2007.
- [10] E. Hairer, C. Lubich, and G. Wanner. *Geometric Numerical Integration*, volume 31 of *Springer Series in Computational Mathematics*. Springer, Berlin, 2nd edition, 2006.
- [11] M. Hasannasab, J. Hertrich, S. Neumayer, G. Plonka, S. Setzer, and G. Steidl. Parseval proximal neural networks. *Journal of Fourier Analysis and Applications*, 26(59):1–31, 2020.
- [12] K. Itoh. Analysis of the phase unwrapping problem. *Applied Optics*, 21(14), 1982.
- [13] P. H. Jones, O. M. Maragò, and G. Volpe. *Optical Tweezers*. Cambridge University Press, Cambridge, 2015.
- [14] A. C. Kak and M. Slaney. *Principles of Computerized Tomographic Imaging*. Number 33 in Classics in Applied Mathematics. Society for Industrial and Applied Mathematics (SIAM), Philadelphia, PA, 2001. Reprint of the 1988 original.
- [15] Z. Kam. The reconstruction of structure from electron micrographs of randomly oriented particles. *Journal of Theoretical Biology*, 82(1):15–39, 1980.
- [16] J. Keiner, S. Kunis, and D. Potts. NFFT 3.5, C subroutine library. <https://www.tu-chemnitz.de/~potts/nfft>. Contributors: F. Bartel, M. Fenn, T. Görner, M. Kircheis, T. Knopp, M. Quellmalz, M. Schmischke, T. Volkmer, A. Vollrath.
- [17] J. Keiner, S. Kunis, and D. Potts. Using NFFT3 - a software library for various nonequispaced fast Fourier transforms. *ACM Transactions on Mathematical Software*, 36:Article 19,1–30, 2009.
- [18] J. Ketola and L. Lamberg. An algorithm for recovering unknown projection orientations and shifts in 3-d tomography. *Inverse Problems and Imaging*, 5(1):75–93, 2011.
- [19] C. Kirisits, M. Quellmalz, M. Ritsch-Marte, O. Scherzer, E. Setterqvist, and G. Steidl. Fourier reconstruction for diffraction tomography of an object rotated into arbitrary orientations. *Inverse Problems*, 37(11):115002, 2021.
- [20] P. Kurlberg and G. Zickert. Formal uniqueness in Ewald sphere corrected single particle analysis. *ArXiv 2104.05371*, 2021.

- [21] M. Kvåle Løvmo, B. Pressl, G. Thalhammer, and M. Ritsch-Marte. Controlled orientation and sustained rotation of biological samples in a sono-optical microfluidic device. *Lab on a Chip*, 21(8):1563–1578, 2021.
- [22] J. C. Lagarias, J. A. Reeds, M. H. Wright, and P. E. Wright. Convergence properties of the Nelder–Mead simplex method in low dimensions. *SIAM Journal on Optimization*, 9(1):112–147, 2009.
- [23] L. D. Landau and E. M. Lifshitz. *Mechanics*, volume 1 of *Course of Theoretical Physics*. Butterworth–Heinemann, Oxford, 3rd edition, 1981.
- [24] M. Moakher. Means and averaging in the group of rotations. *SIAM Journal on Matrix Analysis and Applications*, 24(1):1–16, 2002.
- [25] P. Müller, M. Schürmann, and J. Guck. The theory of diffraction tomography, 2015. ArXiv 1507.00466v3.
- [26] F. Natterer and F. Wübbeling. *Mathematical Methods in Image Reconstruction*. Number 5 in Monographs on Mathematical Modeling and Computation. SIAM, Philadelphia, PA, 2001.
- [27] G. Plonka, D. Potts, G. Steidl, and M. Tasche. *Numerical Fourier Analysis*. Applied and Numerical Harmonic Analysis. Birkhäuser, Cham, 2018.
- [28] D. Schmutz. Reconstruction of projection orientations in cryo-electron microscopy, 2017. Master’s thesis, University of Vienna.
- [29] N. Sharon, J. Kileel, Y. Khoo, B. Landa, and A. Singer. Method of moments for 3d single particle ab initio modeling with non-uniform distribution of viewing angles. *Inverse Problems*, 36(4):044003, 2020.
- [30] A. Singer, R. R. Coifman, F. J. Sigworth, D. W. Chester, and Y. Shkolnisky. Detecting consistent common lines in cryo-EM by voting. *Journal of Structural Biology*, 169(3):312–322, 2010.
- [31] G. Steidl. A note on fast Fourier transforms for nonequispaced grids. *Advances in Computational Mathematics*, 9(3-4):337–353, 1998.
- [32] G. Thalhammer, R. Steiger, M. Meinschad, M. Hill, S. Bernet, and M. Ritsch-Marte. Combined acoustic and optical trapping. *Biomedical Optics Express*, 2(10):2859–2870, 2011.
- [33] M. van Heel. Angular reconstitution: A posteriori assignment of projection directions for 3d reconstruction. *Ultramicroscopy*, 21(2):111–123, 1987.
- [34] M. van Heel, B. Gowen, R. Matadeen, E. V. Orlova, R. Finn, T. Pape, D. Cohen, H. Stark, R. Schmidt, M. Schatz, and A. Patwardhan. Single-particle electron cryo-microscopy: towards atomic resolution. *Quarterly Reviews of Biophysics*, 33(4):307–369, 2000.
- [35] L. Wang, A. Singer, and Z. Wen. Orientation determination of cryo-EM images using least unsquared deviations. *SIAM Journal on Imaging Sciences*, 6(4):2450–2483, 2013.
- [36] E. Wolf. Three-dimensional structure determination of semi-transparent objects from holographic data. *Optics Communications*, 1:153–156, 1969.